Feasibility of Sliding Sealing Vane for Hyperloop Airlock Application

Project Report

Samuel Muirhead[1], Dr Stephen Connolly[1]

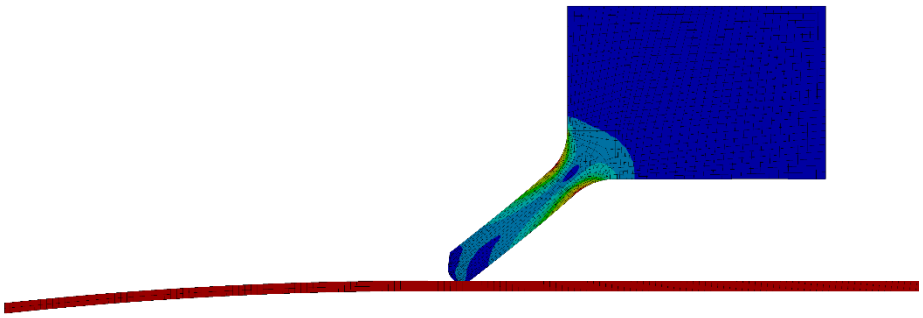

STRATHLOOP

THE CARNEGIE TRUST
FOR THE UNIVERSITIES OF SCOTLAND

[1] Department of Mechanical and Aerospace Engineering, University of Strathclyde, 75 Montrose Street, Glasgow, G1 1XJ

Contents

Table of Figures

List of Tables

Introduction and Background

Hyperloop is a new proposed form of rapid, intercity mass transit. Building on the principles of magnetic levitation, the vehicles, known as pods, travel along a guideway within a low-pressure tube. The vacuum environment reduces aerodynamic drag at high speeds, allowing Hyperloop systems to operate up to the speed of sound.

Due to the pressure differential between the tubes and the atmospheric environment found at Hyperloop stations, an airlock system must be installed. This will allow passengers and cargo to move between the pod internal pressure vessel and the station, without coming into contact with the low-pressure tube environment (P_{tube} ~ 100Pa) which would be harmful to the payload.

This project aims to consolidate the design of a push-through airlock system, in which pods are moved from the vacuum tubes and the platforms using a sealing vane which maintains a temporary seal around the pod body when the main gate valve is open.

Further assessment of the sealing vane will act as a feasibility study for the future development of the airlock system as a whole.

Finite element analysis allows for elements of design to be completed without undertaking physical experimentation.

Initial Project Goals

1. Learn the fundamentals of Explicit finite element analysis
2. Implement learning to create explicit initial simulation
3. Design a sealing vane which is capable of providing a steady state contact pressure of 200 kPa while maximising the fatigue life of the component.
4. Investigate the effects of disturbances on the pod body such as a bump or step.
5. Implement any redesigns to the sealing vane based on the response to the disturbances.

Literature Review

Finite Element Simulations with ANSYS Workbench 14 by H. Lee [1] describes that when analysing the transient behaviour of a structural element, two main types of analyses exist: Implicit and Explicit dynamics. Implicit dynamics is more robust over a larger timestep, however can struggle when strain rates become high. Explicit formulation does not require any convergence at each time step as properties at step n are only dependent upon information from steps n-1, n-2… etc. This allows for more robust simulation of highly dynamic models, but computational times are very long due to the small-time step. Without HCP access, the expected simulation time and time step data for each type of data:

Table 1- Common Simulation Times and Time Step Sizes or Implicit and Explicit Finite Element Formulation

Formulation	Step Size (s)	Simulation Time (s)
Implicit	10^{-3} to 10^{-2}	0.1-10
Explicit	10^{-9} to 10^{-6}	10^{-3} to 1

The robustness and accuracy of an implicit simulation is monitored by force and displacement parameters. The user can set or program control the pass criterion for this factor. For explicit simulation no convergence is required, so an energy error parameter is used to check the accuracy and robustness of the simulation.

It was found that a critical timestep existed where convergence of the model was guaranteed.

$$\Delta t \leq f \frac{h}{c}$$

Where f is a safety factor, h is the smallest element size in the model and c is the wave speed in the material medium, which can be expressed as:

$$c = \sqrt{\frac{E}{\rho}}$$

In a study by L. Shi [2], a back-to-back study was completed on the transient simulation of a car body seal using both explicit and implicit solvers. The study found that both simulations provided generally useful accuracy of the sealing characteristics. However, the explicit simulation was found to be far closer to the experimental data in terms of contact pressure and contact stability.

Studies by Schmidt, Andre and Poll [3], Thatte and Salant [4], [5] and utilised fluid-structure multiphysics to determine the behaviour and performance of a hydraulic rod seal. This method utilised the Reynold's equation for thin fluid films- as shown below- coupled with explicit, transient finite element modelling.

$$\frac{\partial}{\partial \hat{x}}\left(\phi_{xx} H^3 e^{-\hat{\alpha} F \Phi} \frac{\partial}{\partial \hat{x}}(F\Phi)\right)$$
$$= 6\zeta \frac{\partial}{\partial \hat{x}}\left(\{1+(1-F)\Phi\}\{H_T + \phi_{s,c,x}\}\right) + 12\varepsilon \frac{\partial}{\partial \hat{t}}\left(\{1+(1-F)\Phi\}\{H_T + \phi_{s,c,x}\}\right)$$

A study by Martinez et al. [6] utilised fluid structure Multiphysics and an Augmented Lagrangian-Eulerian regime. This method is also used in studies by Gorash, Hamilton and Morrison [7]–[9].

While these methods have been found to be more accurate in modelling seal leakage, technical and computational complexities mean that they were deemed to be beyond the scope of this project.

Yang and Salant [10] investigated the addition of a secondary lip on a hydraulic rod seal for added sealing redundancy. This was found to provide an additional sealing lip when the hydraulic rod experienced a disturbance or a period of high strain (due to a large rod acceleration).

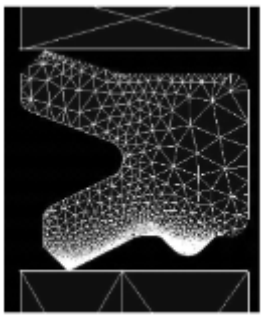

Figure 1- Double Lipped Hydraulic Rod Seal (Yang and Salant [10]*)*

Due to the highly non-linear and incompressible behaviour of elastomer materials, the mathematical modelling of the material behaviour is important to obtaining accurate results. In a study by Ali, Hosseini and Sahari [11], several popular Hyperelastic models were compared to testing data. Each of these models were based on the reduced form polynomial formulation of strain energy for an elastomeric material, as shown below.

$$U = \sum_{i=1}^{N} C_{i0}(\hat{I}_1 - 3)^i + \sum_{i=1}^{N} \frac{1}{D_i}(J_{el} - 1)^{2i}$$

Of these models, the simplest Hyperelastic materials model- Neo-Hookean- was found to be accurate up to strains of 250%. However, in a more in-depth study by Kim et al [12], the Neo-Hookean model was found to be accurate up to strains of 75% for uniaxial loading and pure shear, and experienced inaccuracy at all levels of strain under biaxial loading. The same study found that the Mooney-Rivlin model was accurate on strains of up to 75% in uniaxial loading, 50% in biaxial loading and 250% in pure shear. Finally, the study found that the Ogden model was accurate for all loading types across the full testing strain range (up to 400%). All studies agreed that the determination of the ideal material model to use is highly dependent on the availability of material testing data.

In some studies, including that of Schmidt, Andre and Poll [3], Hyperelastic modelling was not deemed to be enough to give an accurate picture of the material's behaviour. Viscoelastic behaviour models were also added to the material models as the response of elastomer materials is also highly strain rate dependent. Two main forms of viscoelastic material modelling exist: the Prony series and the WLF equation. Viscoelastic properties of Polymers by John D. Ferry [13] provides in-depth fundamental understanding, which is also validated by studies by Kaliske and Rothert [14], Chen [15], Soussou et al [16], Pacheco et al [17], Williams Landel and Ferry [18] and Aubrey and Sherrif [19].

As described in a study by Kaliske and Rothert [14], a simple linear viscoelastic material can be described in terms of a Maxwell element, which combines the characteristics of a Hookean solid and a Newtonian liquid.

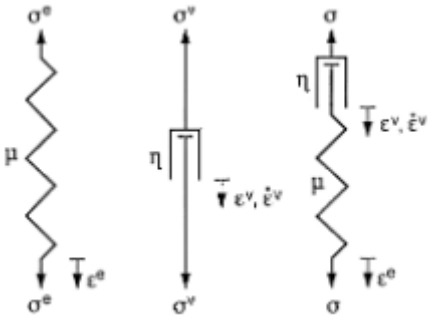

Figure 2- (left to right) Hookean, Newtonian and Maxwellian Elements [14]

This relaxation function can be modelled as a Prony series, as discussed in studies by Chen [15], Soussou et al [16] and Pacheco et al [17]. A basic Prony series is expressed below.

$$\sigma(t) = Y(t)\varepsilon_0$$

Where Y(t) is known as the relaxation function and can be approximated by a Prony series.

$$Y(t) = E_0\left(1 - \sum_{i=1}^{N} E_i\left(1 - e^{\frac{-t}{\tau_i}}\right)\right)$$

The Williams, Landel and Ferry (WLF) Equation [18] is usually expressed in terms of the excitation frequency and the material temperature and describes further the response of an elastomeric material to dynamic loading at different temperatures. This can be added to the Prony series approximation as a temperature shift factor, α_T.

$$\alpha_T = \frac{-C_1(T - T_s)}{C_2 + (T - T_s)}$$

$$Y(t) = E_0\left(1 - \sum_{i=1}^{N} E_i\left(1 - e^{\frac{-t}{\alpha_T\tau_i}}\right)\right)$$

Based on experimental data, the Prony series and WLF equation constants can be calculated either by analytical methods (Aubrey and Sherriff [19]) or by numerical methods (Chen [15]). Numerical methods are used more commonly in modern finite element models,

Rubber Formulary by Cuillo and Hewitt [20] has a large amount of viscoelastic data on different elastomer materials, as does software PolyUMod.

Non-linear viscoelastic affects were studied by Drozdov [21], but these models were considered beyond the scope of the project.

Another important part of the sealing vane finite element model will be the contact interactions between the pod body and sealing vane. Studies by Malachowski et al [22] and Yang, Deng and Li [23], both utilised the pure penalty contact formulation in Explicit dynamics software LS-DYNA. Within LS-DYNA, two types of contact detection algorithms exist- node-to-segment and segment-to-segment algorithms. In the study by Malachwoski et al [22], both of these contact formulation methods were found to be suitably accurate.

A minimum explicit time step to ensure contact stability is discussed in the study by Yang, Deng and Li [23].

$$\Delta t \leq min\left\{\frac{m^j}{k}\right\}$$

Where m is the mass of the body attached to the contact spring (slave body), k is the stiffness factor of the pure penalty method and j is either 1 or 2, whichever gives a minimum. It is indicated by this study that the smaller of the two critical time step values shall be used in the explicit simulations.

The study by Malacowski et al [22] also indicated that the mesh element sizing around the contact surfaces shall be no greater than 5% of the minor axis length of the contact patch. Both studies found more accurate results by making the body with the lower mesh density the master body. Handbook of Contact Mechanics by Popov et al [24] give a fundamental understanding and analytical solutions to axisymmetric contact problems.

Explicit Workflow

The first key goal of the project was to produce an accurate mathematical model to represent the sealing vane system in a computationally efficient manner.

Based on the literature review, a basic explicit finite element model was created to understand the explicit simulation workflow within the LS-DYA plugin of ANSYS workbench.

Geometry

As the Hyperloop pod and tube are symmetrical around the vast majority of their circumferences, a 2-dimensional axisymmetric approximation was used. This meant that the number and complexity of elements was significantly reduced with a small reduction in the overall accuracy.

In the physical model, the fixing points on the base of the vane would be supported by a metal casing which runs the circumference of the sealing vane. As the metal is significantly more rigid than the rubber vane material, a fixed support was used on the surfaces of the vane connected to the casing. Therefore, there was no need to model the casing in the mathematical model, further reducing the required number of elements in the mathematical model.

As the analysis to be conducted in all explicit cases is transient, the pod body geometry was shortened to cover the settling time of the vane on its surface. It was found that a 1 metre sliding distance was suffice in the case of the initial simulation- however this was changed in other simulations with a longer settling time. This was deemed a valid simplification as once the vane has reached a steady state, the values of stress, strain and contact pressure would all remain constant with any future simulated time.

The pod body was also simplified to only include the body shell layer in the analysis. This further reduces the number of elements required while still providing the pod surface for the vane to contact. Figure 3 shows a 2D section of the physical model and Figure 4 shows a sketch of the 2D geometry used in the analysis.

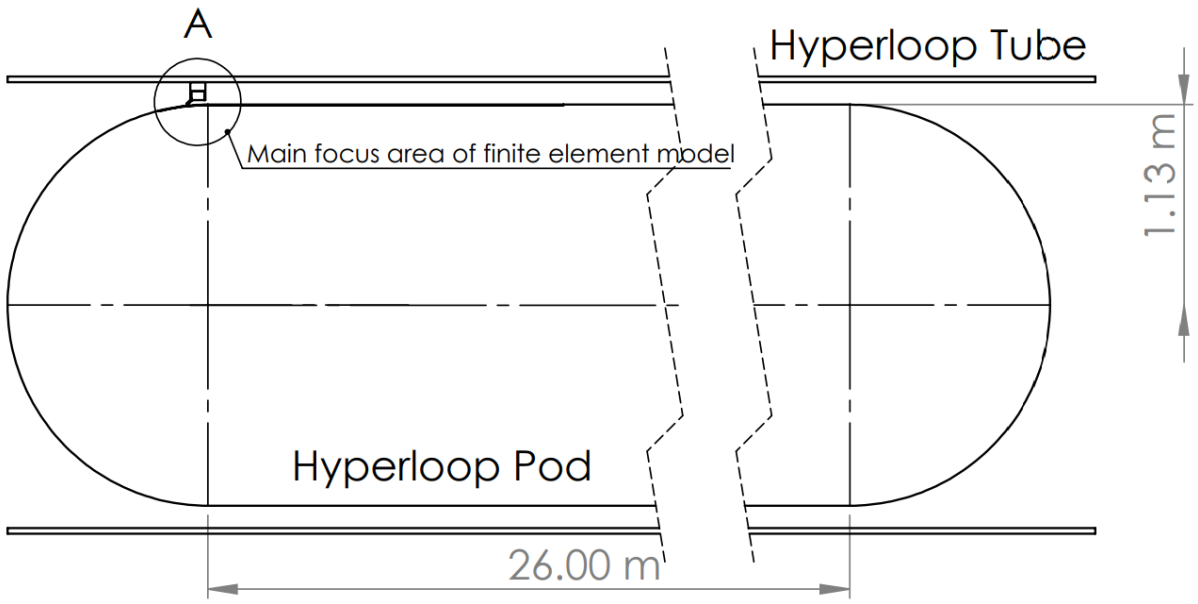

Figure 3- General Sketch of Hyperloop Pod-Vane Interaction

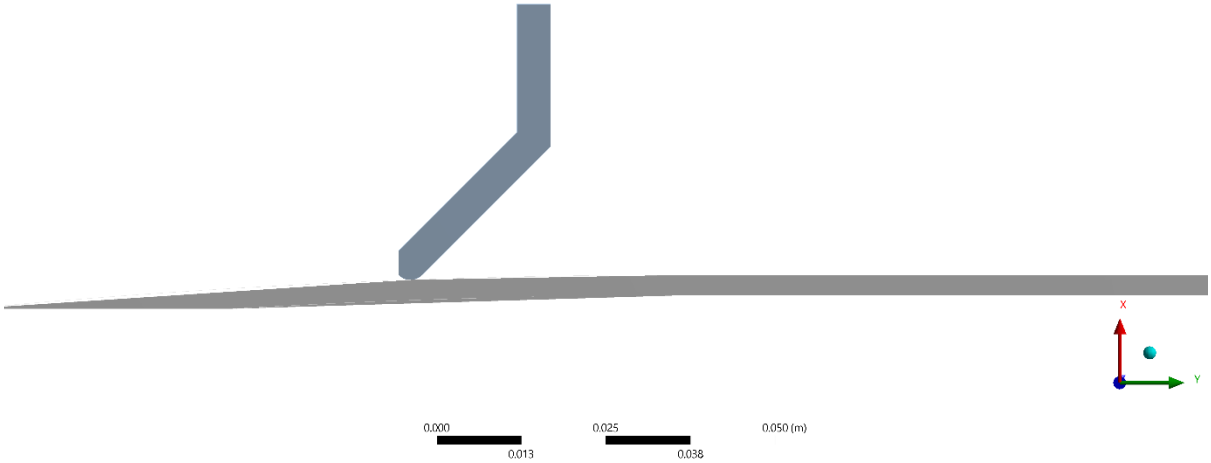

Figure 4- Geometry Domain of Initial Explicit Simulation

Engineering Data

Table 2 shows the key material data used in the model.

Table 2- Material Data for Explicit Simulation

Sealing Vane		
Parameter	Value	Units
Density	1500	kg/m^3
Elastic Modulus	5	MPa
Poisson's Ratio	0.4999	N/A
Pod Body		
Density	72,115	kg/m^3
Elastic Modulus	71	GPa
Poisson's Ratio	0.334	N/A

To simplify the initial simulation, the Hyperelastic model was replaced with a linear elastic model will a very high Poisson's ratio. This would help reduce some of the non-linearity from the simulation. The pod body was assumed to be aluminium. The density of the material was scaled such that the mass of the pod body was 15 tons, a rough approximation of the weight of a full-scale Hyperloop pod.

Discretisation

The geometry domain was discretised using explicit linear 2D elements. As the required time step is linked to the size of element, initially the size of the elements was to be kept as large as possible to minimise the computational cost of the initial simulations. The initial mesh can be seen in Figure 5 with the key statistics shown in Table 3.

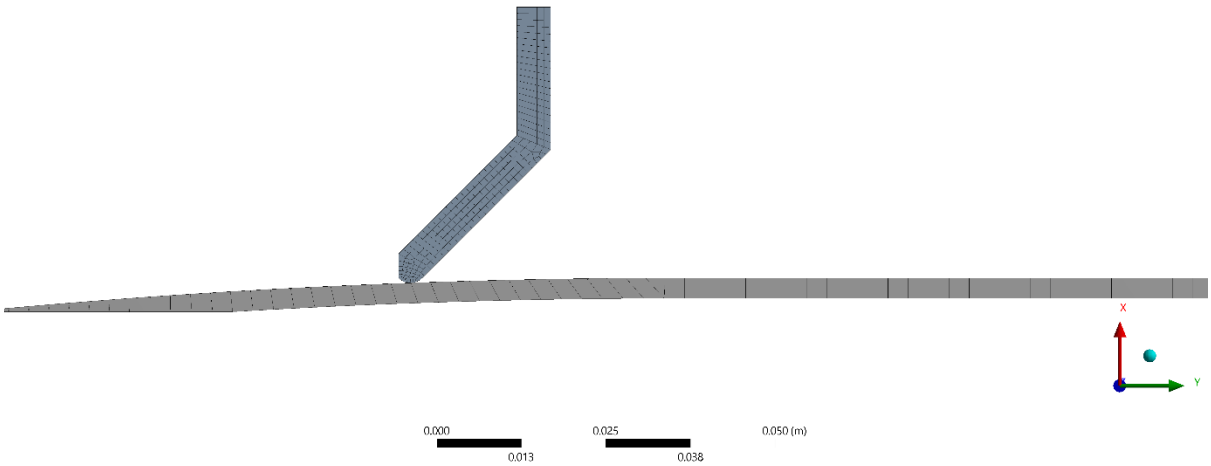

Figure 5- Mesh of Geometry Domain for Explicit Initial Simulation

Table 3- Mesh Statistics of Explicit Initial Simulation

Parameter	Number of Nodes	Number of Elements	Maximum Skewness	Minimum Element Quality
Value	1063	636	0.86	0.16

Boundary Conditions

Firstly, an initial condition for the pod velocity was set to 5m/s to simulate the approach of the pod to the sealing vane. The pod was constrained to move in only the axial direction by a frictionless support placed at the bottom of the pod body geometry.

The sealing vane was held in place using a series of fixed supports- as discussed in the geometry section. These supports were placed on the surfaces of the vane which would be in contact with the casing. The boundary conditions used on the model are shown in Figure 6.

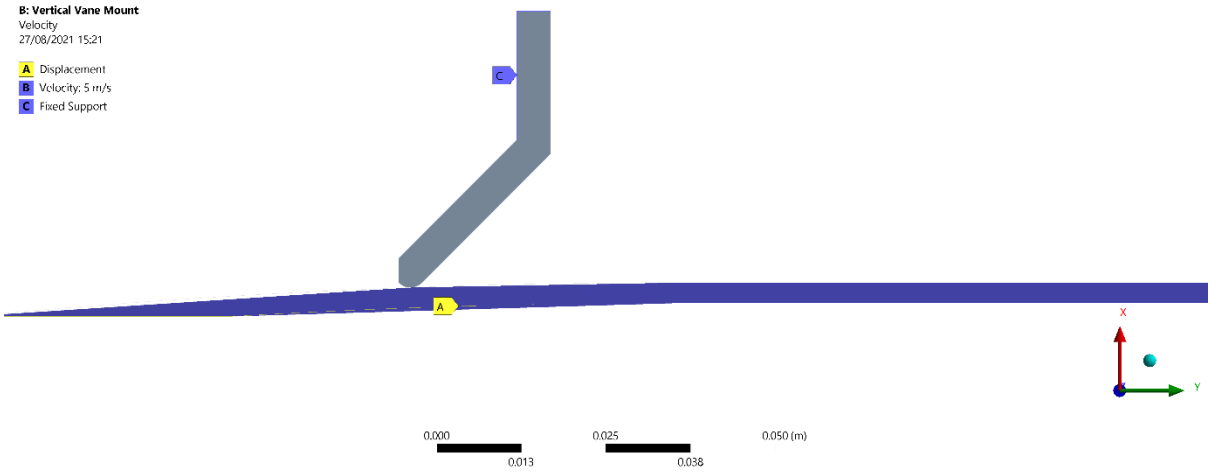

Figure 6- Boundary and Initial Conditions of Explicit Initial Simulation

A frictional contact region was setup between the pod body top surface and the bottom of the vane, as shown in Figure 7. Due to the pod body being far more rigid than the sealing vane, and thus the deformation due to contact being very asymmetric, an asymmetric contact formulation was selected. This meant that all the contact formulation was calculated on the sealing vane side.

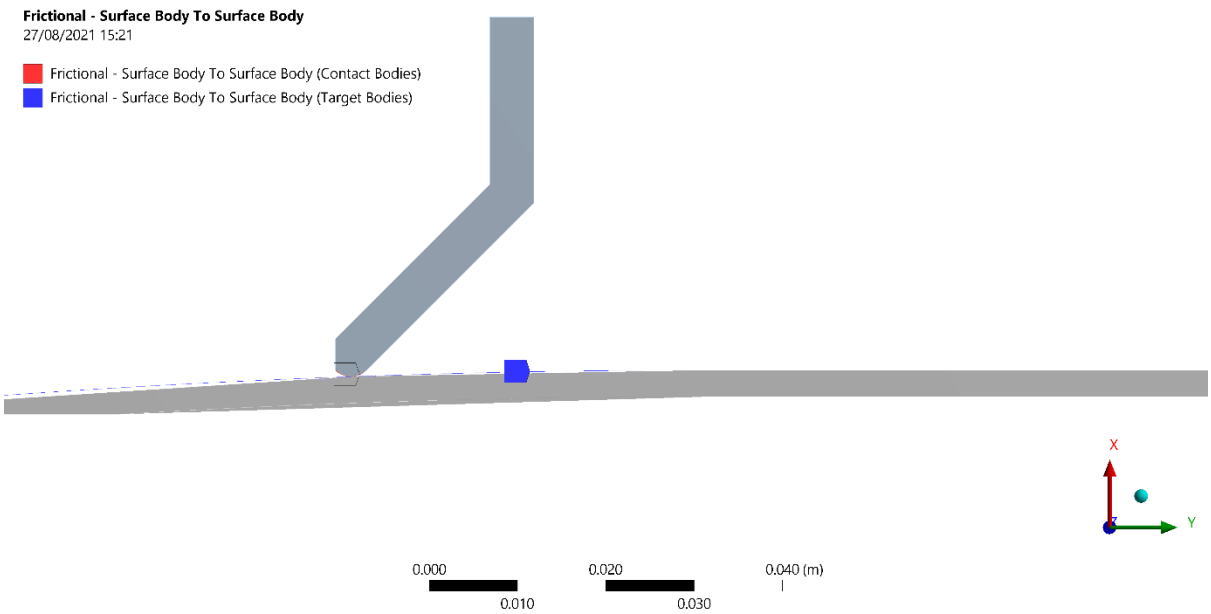

Figure 7- Contact Surface Assignment of Explicit Initial Simulation

Initial Results

The results of the simulation are shown in Figure 8 to Figure 10.

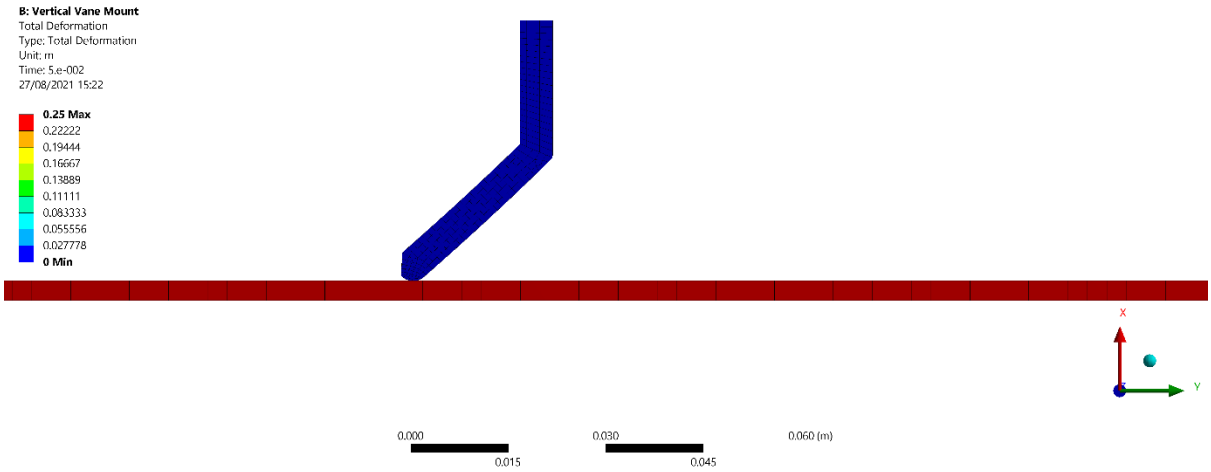

Figure 8- Total Deformation Plot of Initial Explicit Simulation

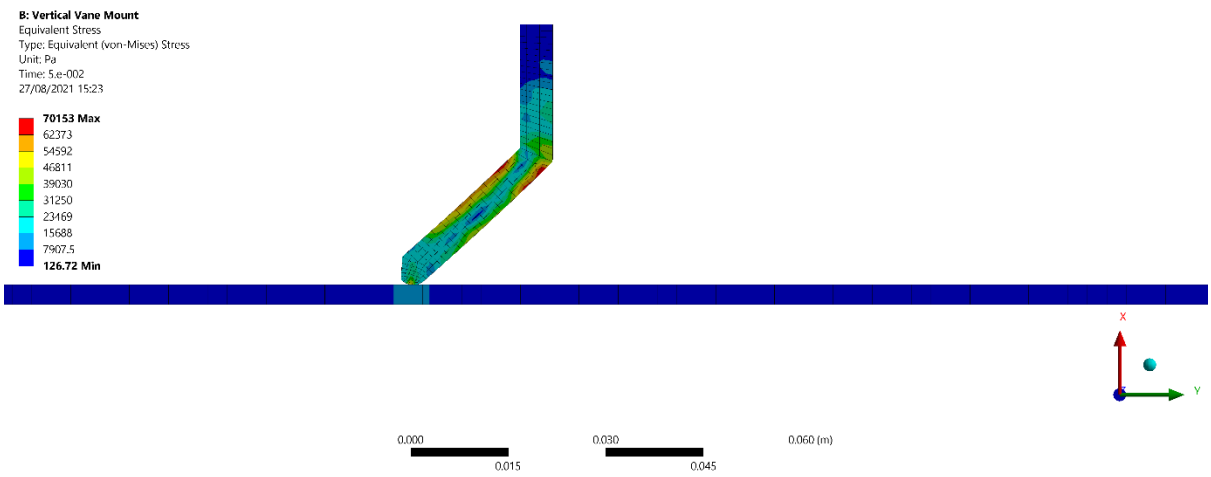

Figure 9- Von Mises Equivalent Stress Plot for Initial Explicit Simulation

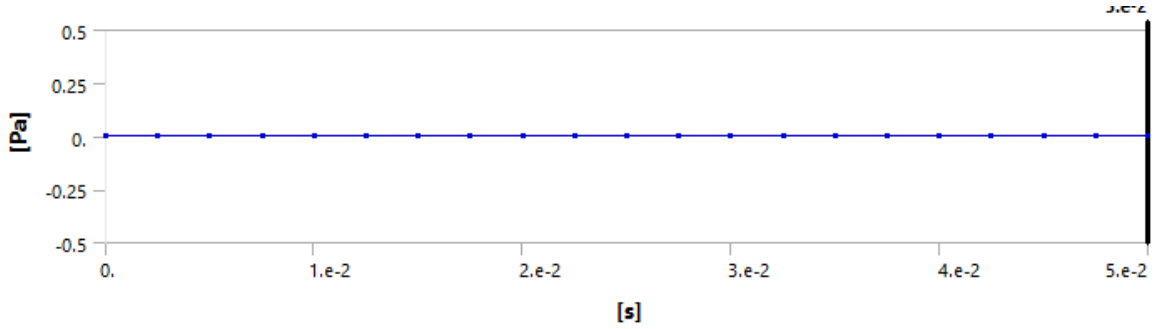

Figure 10- Contact Pressure Results Graph from Initial Explicit Simulation

The lack of contact pressure results was a major concern as these results were to be used substantially as a performance indicator of the sealing vane. This was found to be due to an incompatibility in the LS-DYNA plugin of ANSYS workbench and that the pre-processor does not write 2-dimensional contact keywords to the input file. This means that the results will not contain any contact pressures.

Manual Keyword Editing

ANSYS LS-DYNA allows the exportation of the LS-DYNA input file from the workbench project. A workflow was devised as shown in Figure 11.

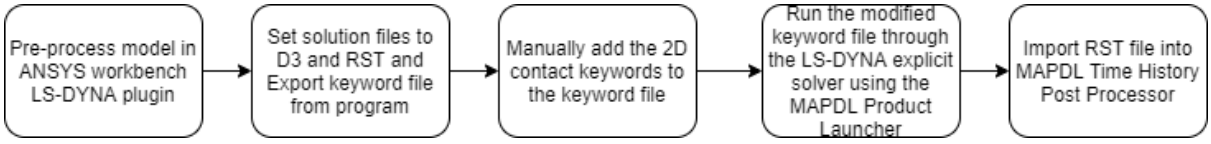

Figure 11- Potential Manual Keyword Editing Workflow for 2D Contact in ANSYS DYNA

The workflow was proven to be successful, as the stress and strain results were successfully viewed using MAPDL post-processor. However, the keyword editing was not successful within the timeframe given in the project.

Furthermore, the complexity of the file management to produce results would rule out any design optimisation- and thus limit the scope of the project even further.

Discussion

For the reasons stated above, it was decided that the explicit solver parts of the project analysis would not be completed within the scope of the project.

Instead, the implicit model would be carried forward and more of the project's scope would be focussed on the design optimisation of the steady state case. The new project goals are listed below:

1. Create an initial finite element model using implicit method for solution.
2. Achieve mesh convergence of this model by performing a mesh refinement study.
3. Use design optimisation to design a sealing vane which can provide a steady state contact pressure of 200 kPa while maximising the fatigue life of the component.
4. Investigate the robustness of the optimised sealing vane to changes in pod approach velocity and co-efficient of friction.
5. Investigate the effects of disturbances on the pod body such as a bump or step.

Implicit Simulation Setup

As the implicit method was well known to the Author, no further research was deemed necessary to continue with the implicit simulation. The key assumptions of the explicit finite element model were carried forward to the implicit model.

Engineering Data

The material data for the pod body and sealing vane can be seen in Table 4.

Table 4- Material Data of Sealing Vane and Pod Body

Sealing Vane		
Parameter	Value	Units
Density	1500	kg/m^3
Initial Shear Modulus	5	MPa
Incompressibility factor	0	N/A
Pod Body		
Density	72,115	kg/m^3
Elastic Modulus	71	GPa
Poisson's Ratio	0.334	N/A

A Neo-Hookean Hyperelastic model was used in the mathematical model as it minimised the complexity of potential optimisation as it contained only 1 stiffness parameter and an incompressibility factor. The same material was used for the pod body as the explicit simulation.

Geometry

A similar geometry to that of the explicit simulation was created for the implicit model. Some changes were made the way the model was constrained to reduce the number of input parameters for design optimisation. A sketch of the model is shown in Figure 12 and the modelled geometry within the ANSYS platform is shown in Figure 13.

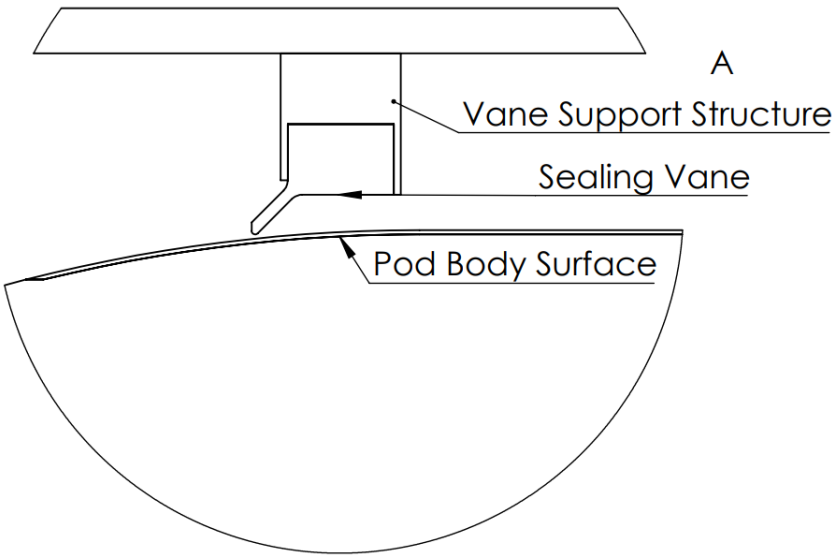

Figure 12- Detailed View of Focus Area of Finite Element Model

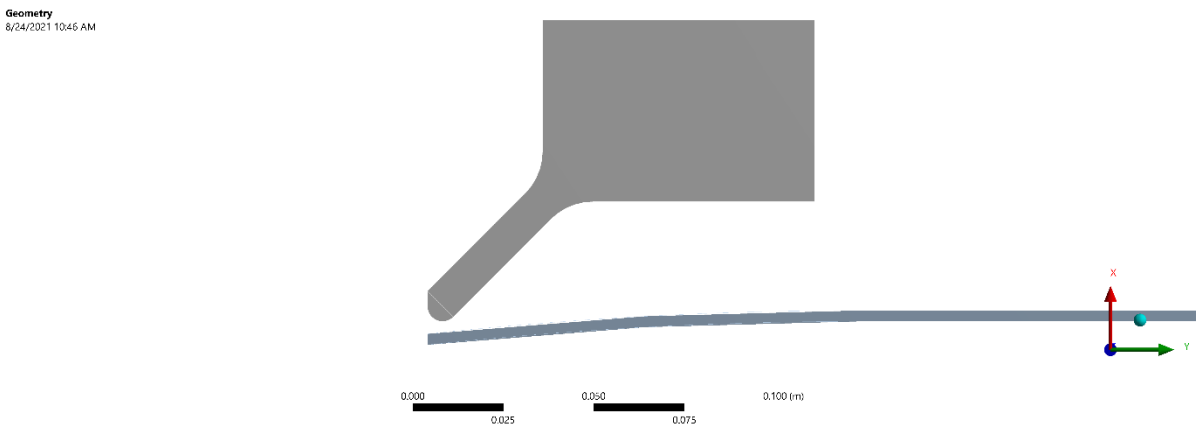

Figure 13- Geometry of Sealing Vane and Pod Body

The model was constrained in a way which would ease the integration of design optimisation later in the project. The main geometric parameters created in the model to be optimised were the vane thickness, compression and sweep angle.

The top of the vane base was constrained to be 1.15m as per the minimum support clearance determined in the author's previous work in the subject.

Discretisation

The goal was the refine specific areas of the geometry in order to aid the speed of sub step convergence and decrease the solution time. The key areas requiring refinement was the vane contact surface and the anticipated area of maximum stress at the base of the vane. The model was split into different segments for meshing as shown in Figure 14. Where possible, quadrilateral block structured face meshing was used to minimise the skewness of the model. During discretisation, mechanical 2nd order elements were created. The finalised mesh can be seen in Figure 15, along with the skewness distribution graph in Figure 16.

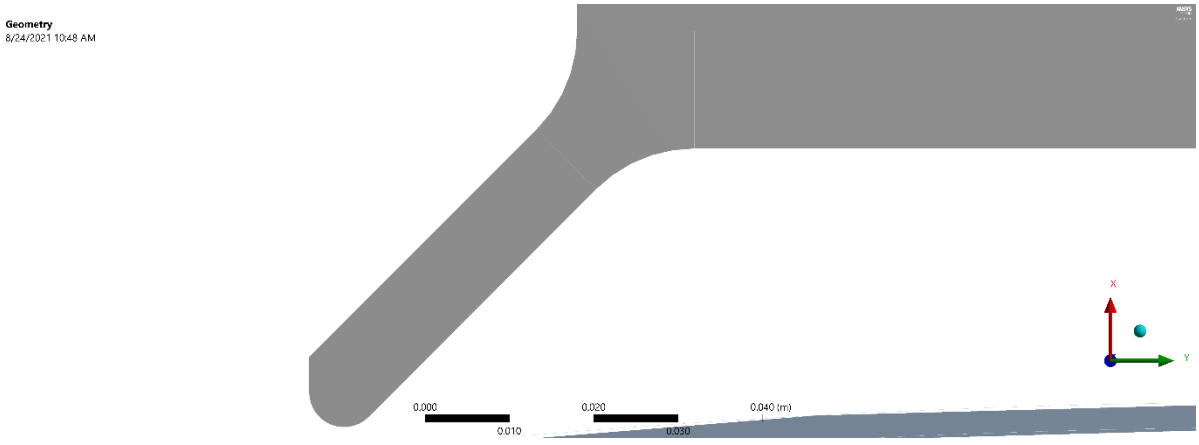

Figure 14- Sealing Vane Geometry Areas for Block Structured Meshing

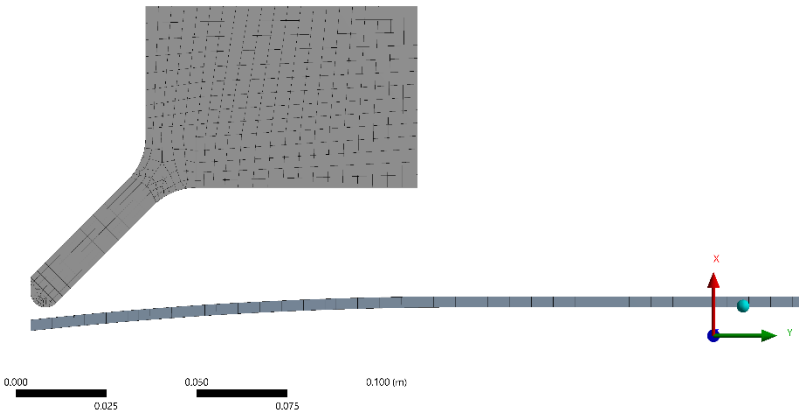

Figure 15- Initial Mesh of Geometry Domain for Implicit Formulation

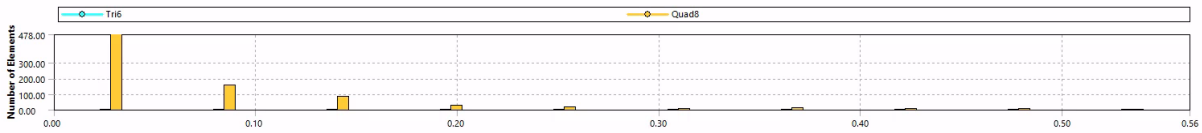

Figure 16- Skewness Distribution for Initial Implicit Mesh

Table 5 shows the statistics of the discretised model.

Table 5- Mesh Characteristics of Implicit Formulation

Parameter	Number of Nodes	Number of Elements	Maximum Skewness	Minimum Element Quality
Value	3193	779	0.56322	0.51695

Boundary Conditions

The initial and boundary conditions discussed can be shown highlighted in Figure 17- these are akin to the conditions used previously in the explicit model.

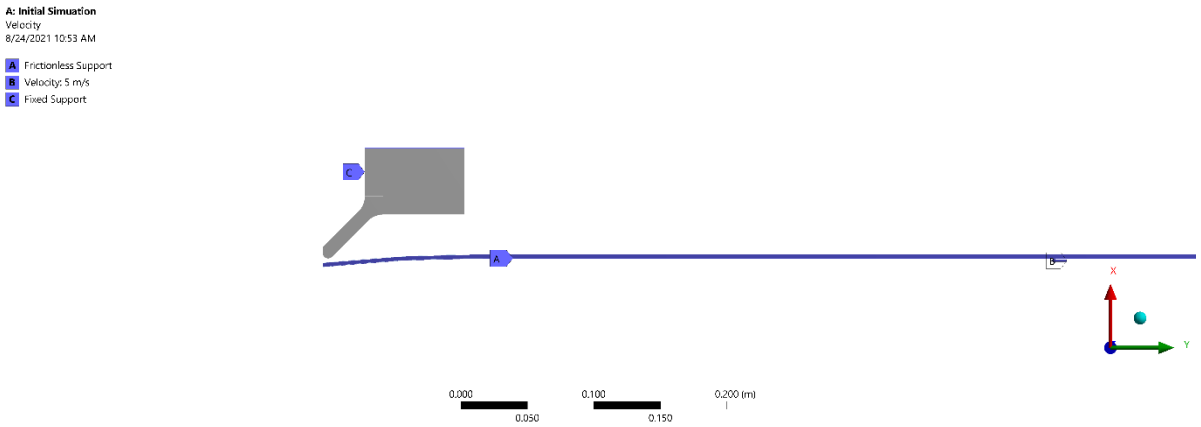

Figure 17- Boundary Conditions in Initial Implicit Finite Element Model

Similar to the explicit model, an asymmetric contact region between the pod body and vane was generated. The assignment of contact surfaces is shown in Figure 18.

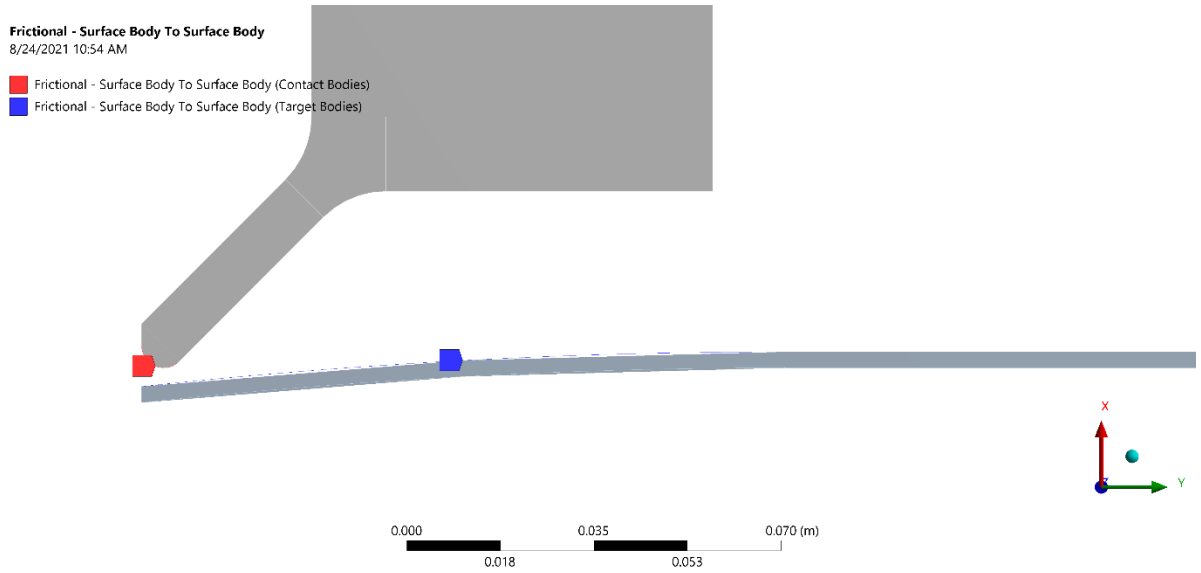

Figure 18- Frictional Contact Region Sealing Vane to Pod Body

Analysis Settings

The analysis settings used in the model is shown in Table 6

Table 6- Analysis Settings of Implicit Simulation

Simulation Time	Initial Time Step	Minimum Time Step	Maximum Time Step	Newton Raphson Method	Energy Dissipation Ratio
0.2s	4e-04s	5e-05s	0.001	Asymmetric	1.00E-04

Initial Results

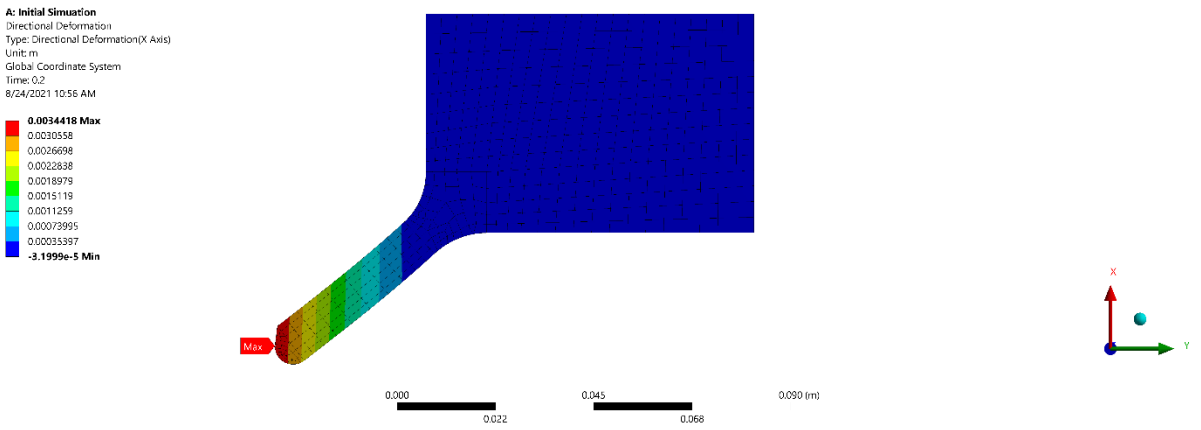

Figure 19- Steady State Radial Deformation of Sealing Vane Component (True Scale)

Figure 19 shows that the radial deformation reached a maximum of 3.44mm. Considering the Vane Compression was set to 3mm for this simulation, this result showed that the vane was deforming as expected due to the contact.

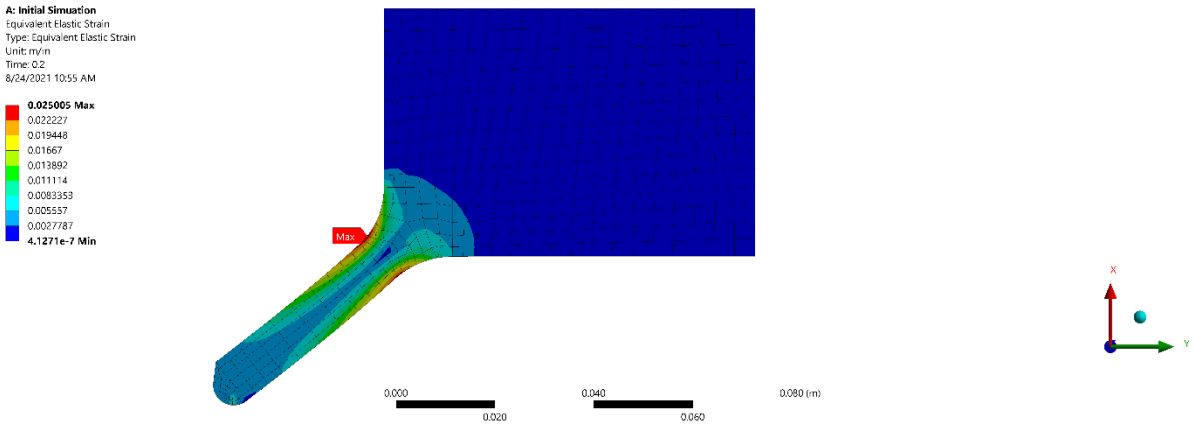

Figure 20- Steady State von Mises Equivalent Strain of Sealing Vane

Figure 20 shows that a maximum strain of 2.5% was found at the areas around the base of the extended surface of the sealing vane, with the maximum strain points being at the edges of the model. This shows that the friction from the sealing vane operated correctly as the vane extended surface acts as if it undergone bending. This phenomenon was also observed in the stress plot, with a maximum of 374.94 kPa occurring at the sim point as the point of maximum strain- as shown in Figure 21.

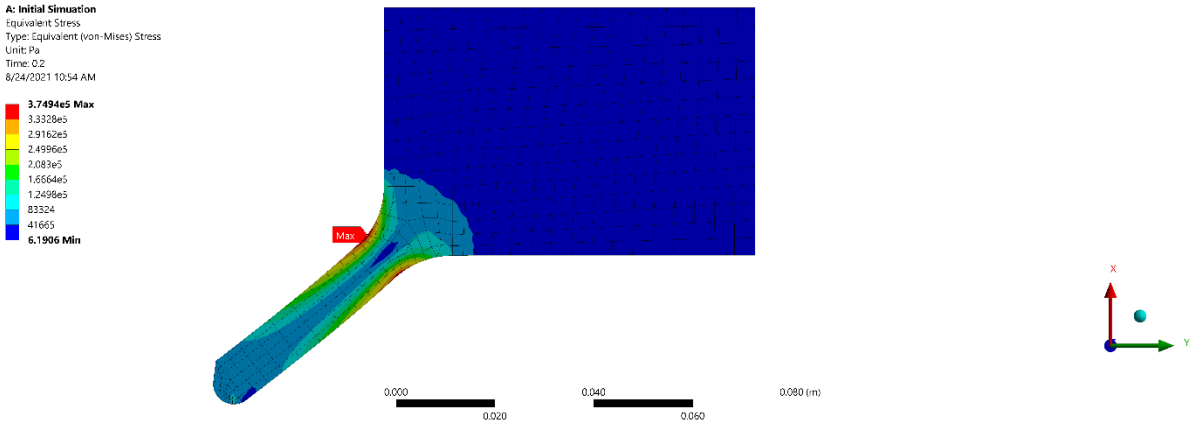

Figure 21- Steady State von Mises Equivalent Stress of Sealing Vane

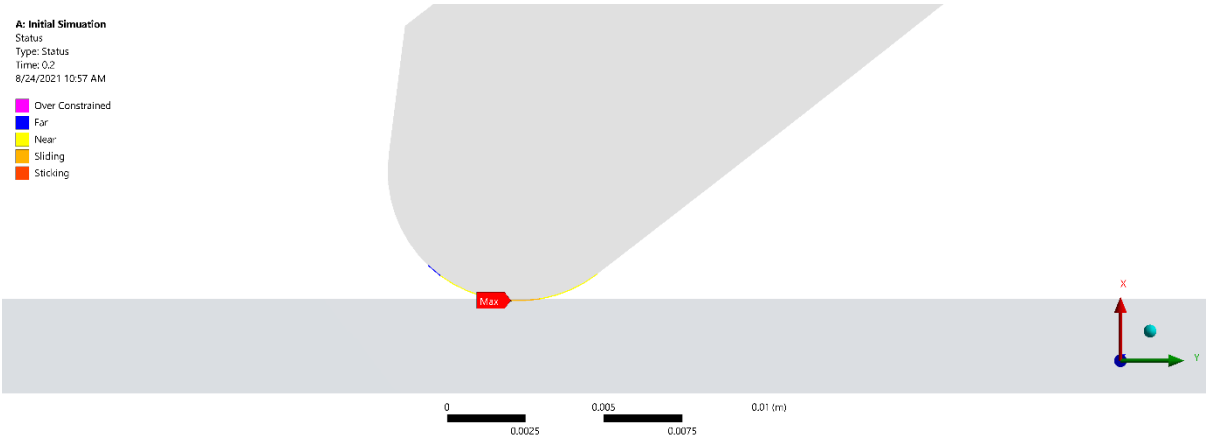

Figure 22- Sealing Vane and Pod Body Steady State Contact Status

Figure 22 shows that the contact was initiated during the simulation and that sliding friction occurred as was desired from the component interaction. Figure 23 shows that a maximum model penetration of 50µm occurred in the centre of the contact area. This distribution can be characterised as a Hertzian distribution, a well-established contact parameter distribution.

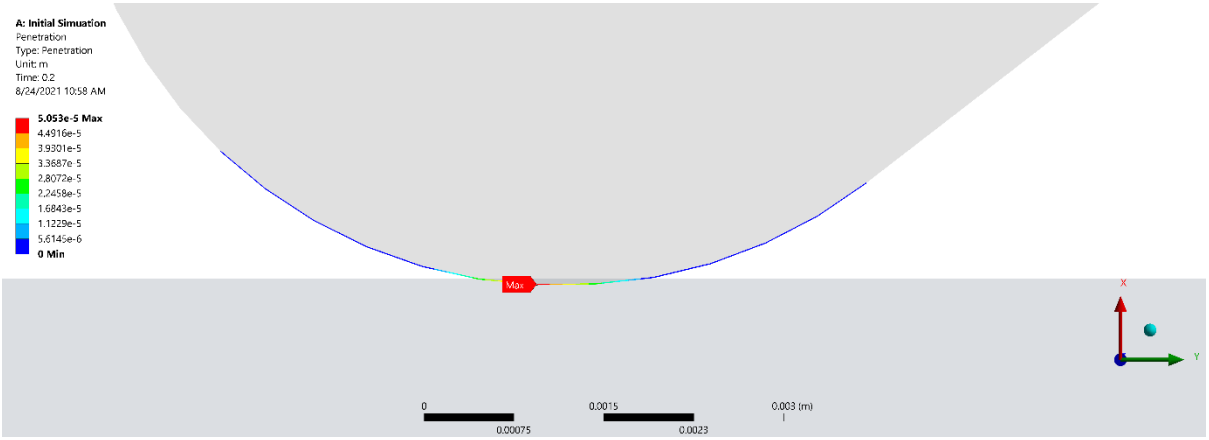

Figure 23- Sealing Vane and Pod Body Steady State Contact Penetration Distribution

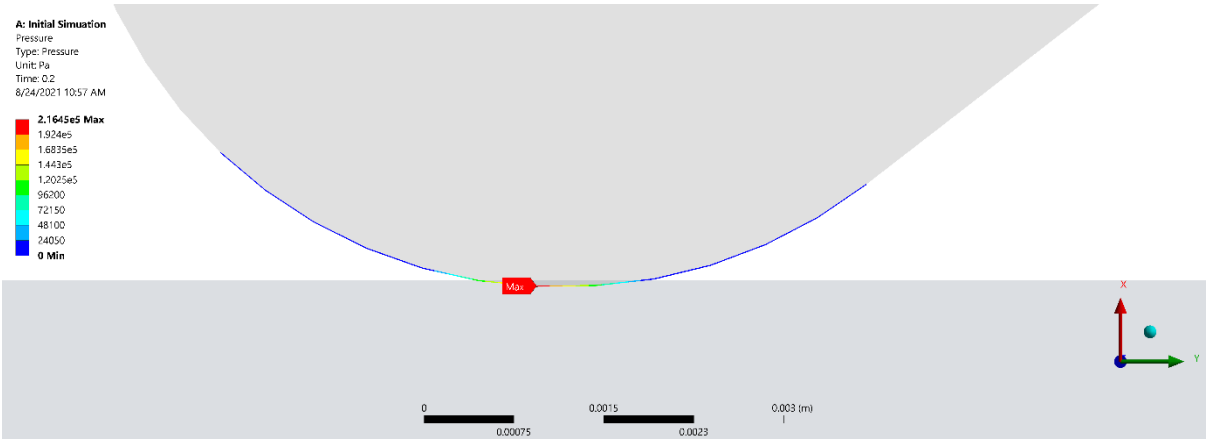

Figure 24- Sealing Vane and Pod Body Steady State Contact Pressure Distribution

Figure 24 shows that the contact pressure also followed a Hertzian distribution, with a maximum value of 216.45 kPa found at the centre of the contact area. Figure 25 shows the time history of the contact pressure result. The contact pressure was observed to spike to a maximum of 269.42 kPa on

impact, followed by a decaying period of sinusoidal oscillation which converges on a steady state value of contact pressure.

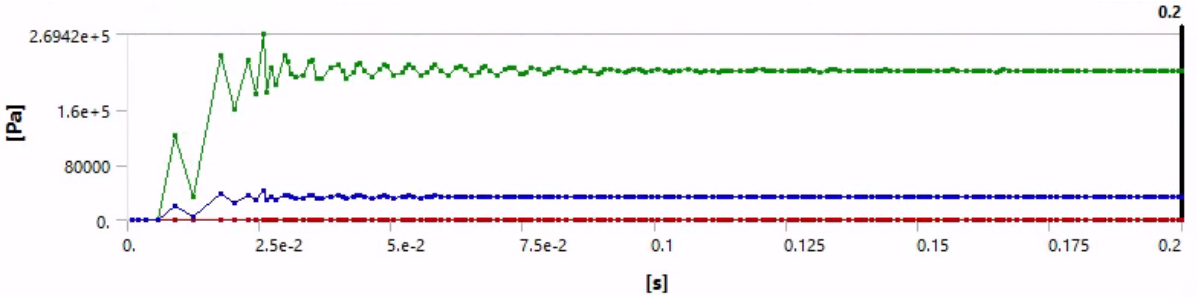

Figure 25- Time History of Contact Pressure Result in Implicit Formulation

Following the generation of this initial model, the next step was to ensure numerical validation of the discretisation and analysis settings by means of a mesh refinement study.

Mesh Refinement Study

In order to validate that the discretisation required for numerical solution provided an robust approximation of the continuum domain, convergence of output variables by changes in mesh density was sought. This process would allow results to be more reliable for comparing to experimental data in further work.

Convergence in this case was defined when the percentage rate of change per percentage refinement reduced below 5%, as expressed below:

$$\frac{ds}{dn} = \frac{\%change\ in\ Ouptut\ Variable}{\%change\ in\ Number\ of\ Elements} \leq 0.05$$

This criterion was mathematically modelled in MATLAB to allow for instant analysis of convergence data. The MATLAB script can be found in Appendix 1. The key output parameters of interest were the steady state maximum contact pressure and steady state maximum equivalent von Mises stress values, these stress/strain values and contact values would be used later in design optimisation

Global Refinement

Firstly, a global mesh refinement study was conducted- whereby all mesh sizing operations were altered at a similar rate of refinement at each refinement step. The results of this study are shown in Figure 26 to Figure 29.

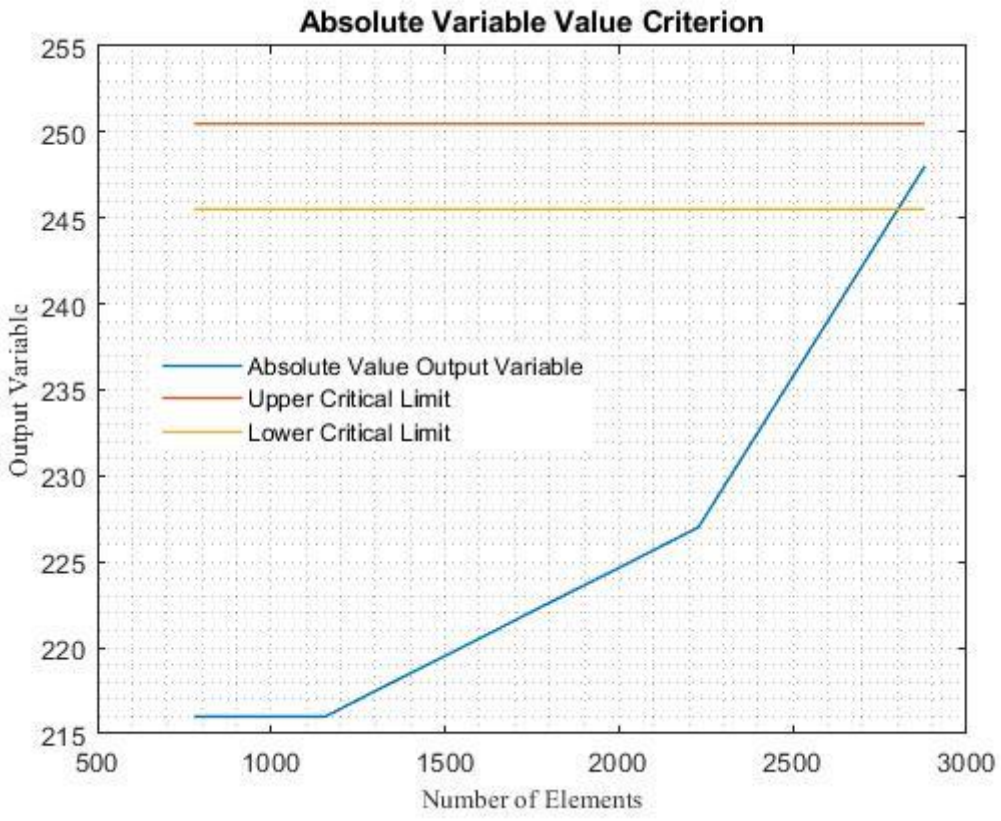

Figure 26- Absolute Value Plot of Steady State Maximum Contact Pressure vs Number of Model Elements

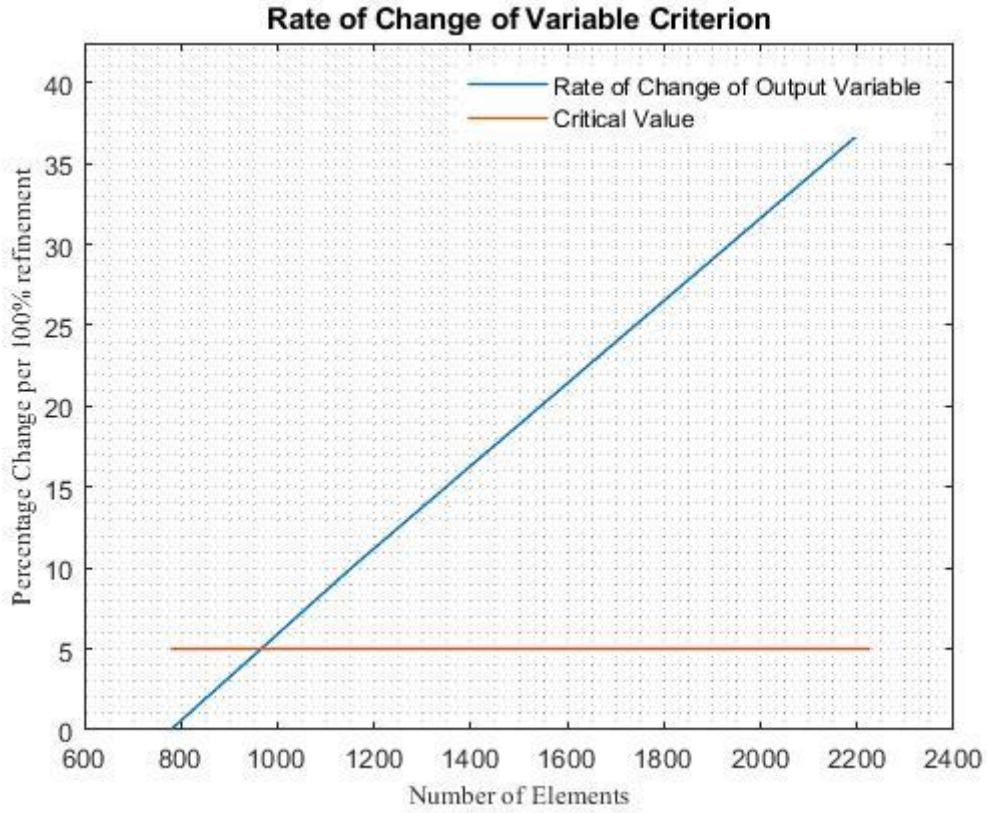

Figure 27- Rate of contact pressure change vs number of model elements

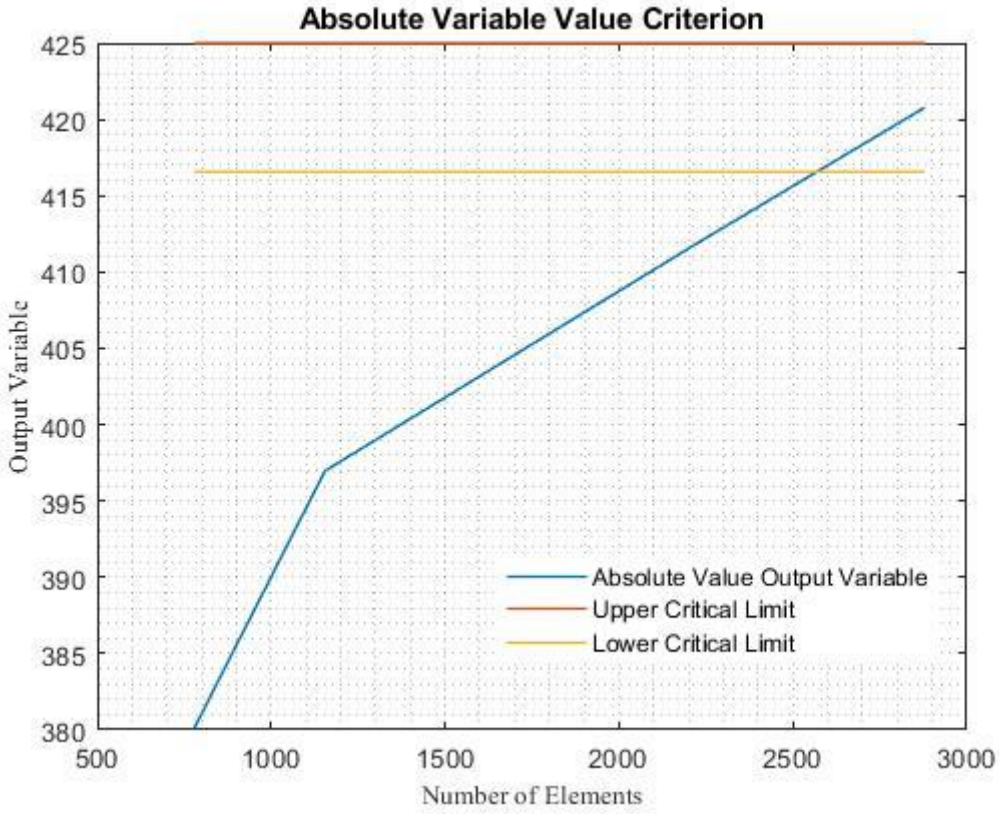

Figure 28- Absolute Value Plot of Maximum von Mises Equivalent Stress vs Number of Model Elements

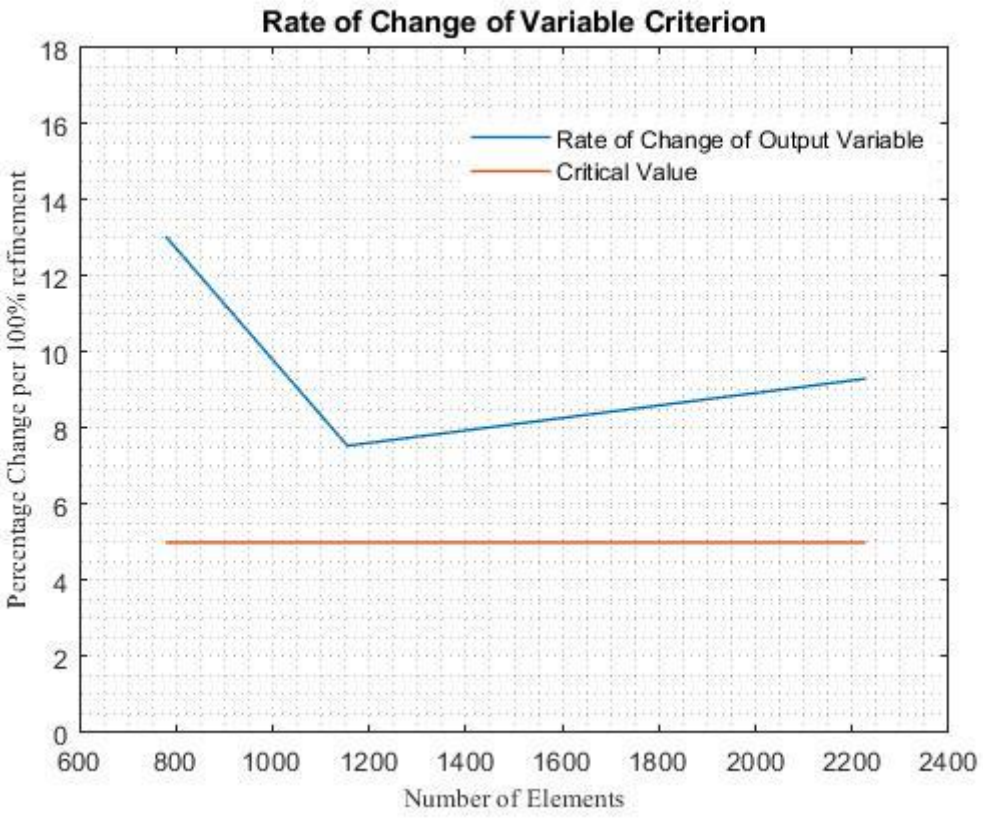

Figure 29- Rate of stress change vs Number of Model Elements

Neither the stress of contact pressure results showed characteristics of convergence during this study. The contact pressure convergence worsens as the mesh is further refined. The lack of stress convergence at this stage was a little unexpected, but this was put down to the increase in force on the vane from the sharply increased contact pressure.

Based on this study, the need for a series of local refinement studies to better understand the characteristics of the model was clear. 3 main areas of the model were chosen to be focussed on- the contact surface of the pod body, the area of maximum stress in the vane and the contact surface of the vane. Once local convergence was found at these 3 points, overall convergence could be assured.

Local Refinement Study- Pod Body Contact Surface

While the asymmetric contact formulation should mean that the pod element size should not affect the output parameters, it was decided that this was to be checked. The results of the study can be found in Figure 30 to Figure 33.

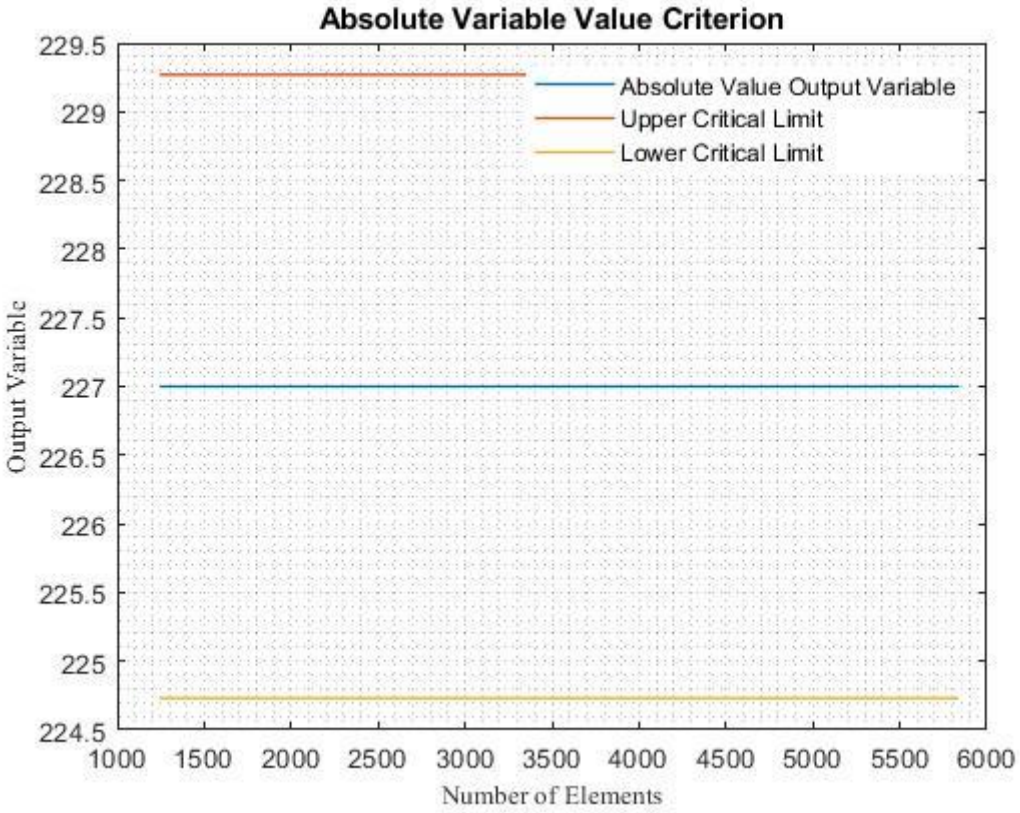

Figure 30- Absolute value plot of Contact Pressure vs Number of Pod Elements

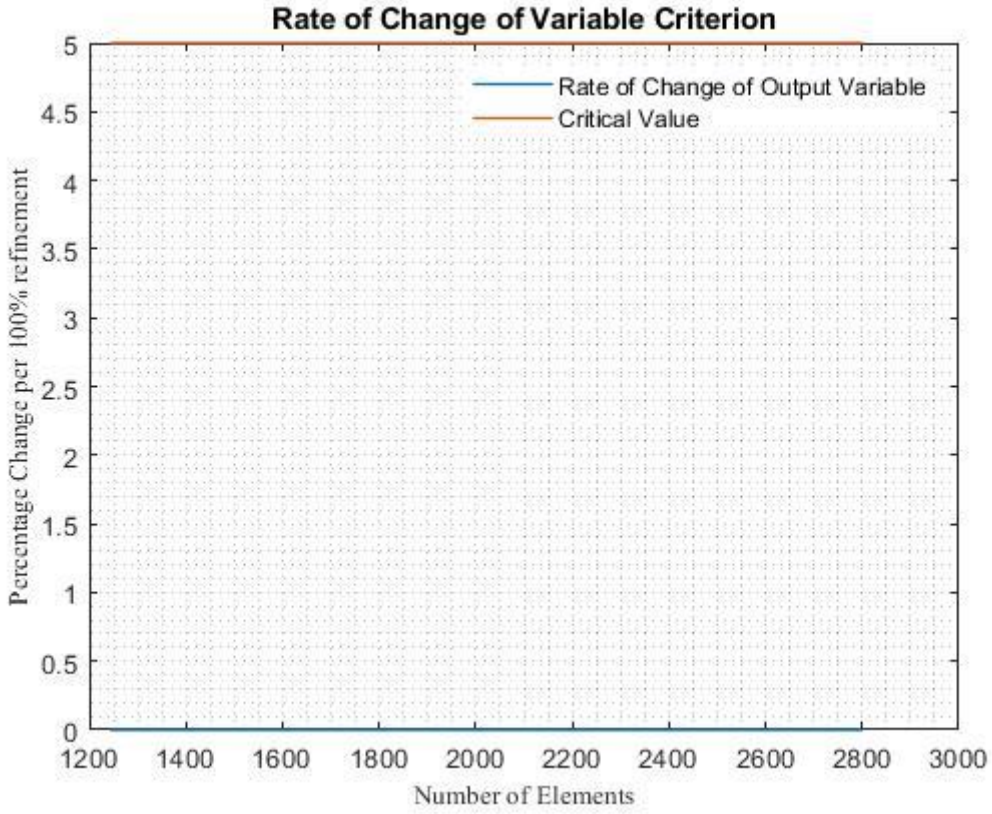

Figure 31- Percentage Rate of Change of Contact Pressure vs Number of Pod Elements

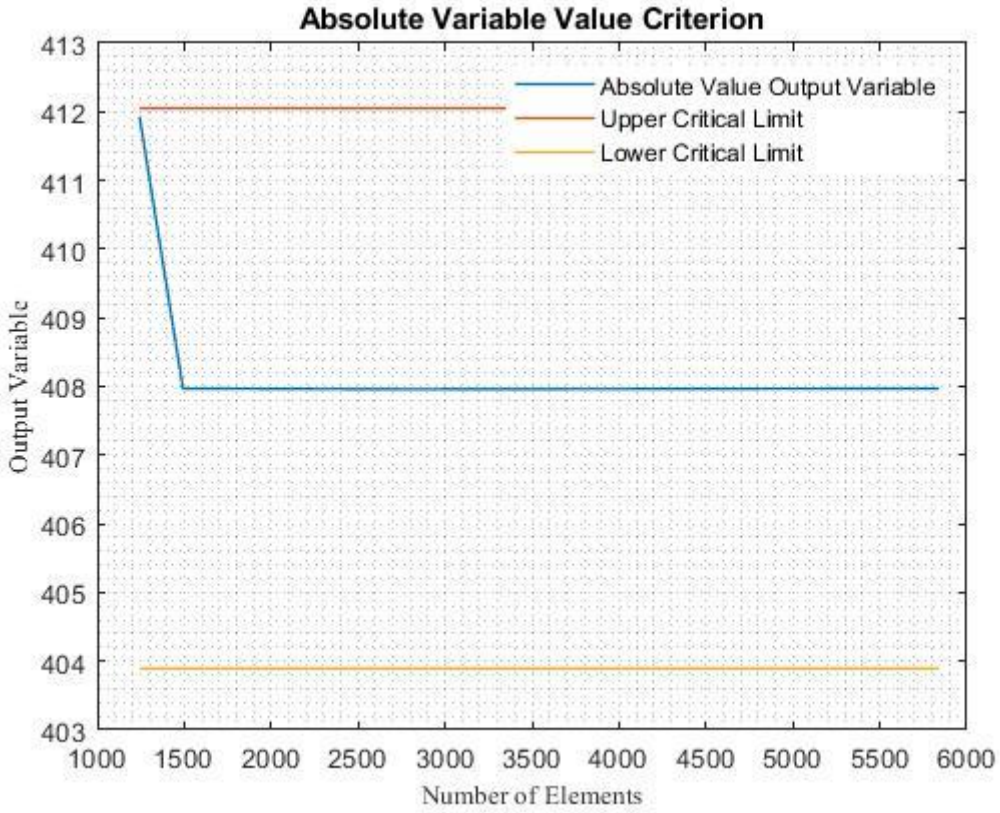

Figure 32- Absolute Value of Maximum von Mises Equivalent Stress vs Number of Pod Elements

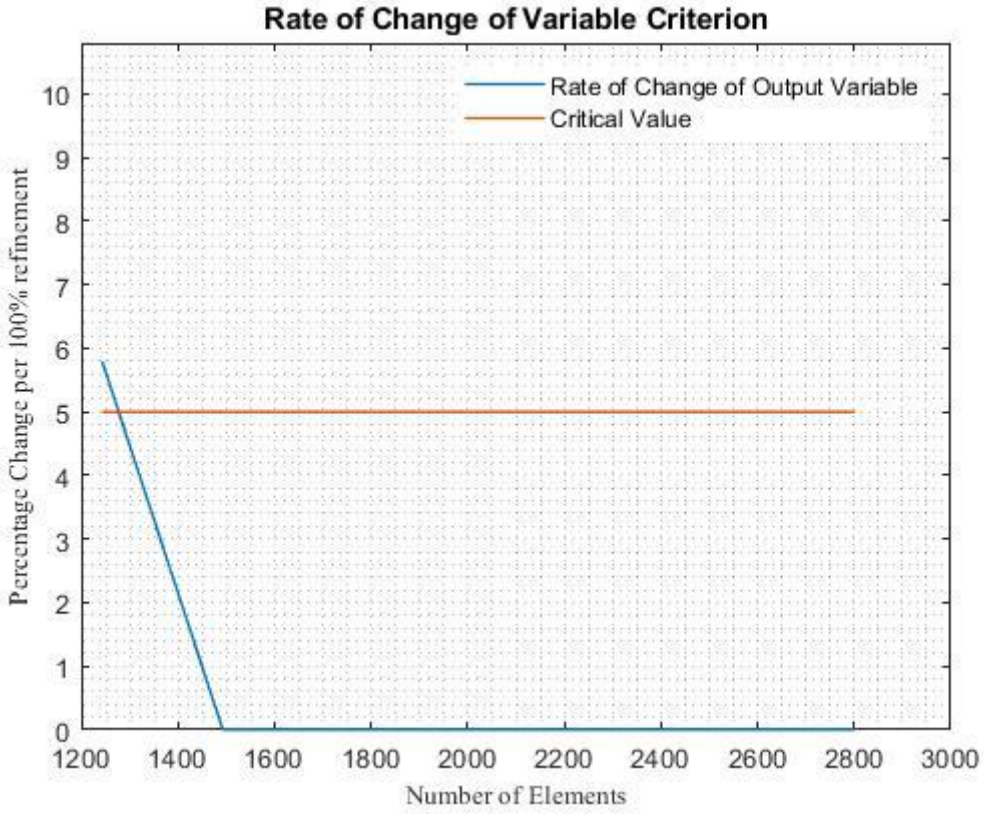

Figure 33- Percentage rate of change of Maximum von Mises Equivalent Stress vs Number of Pod Elements

As was expected, changing the pod element size had no effect on the results of the simulation, and thus a robust local refinement convergence was achieved.

Local Refinement Study- Area of Maximum Stress

As is common with many mesh convergence studies, this local refinement study focussed on the point of maximum vane stress. From the initial simulation, this was found to be in the curved section between the finger of the vane and the base of the vane.

The results of the study are shown in Figure 34 and Figure 35.

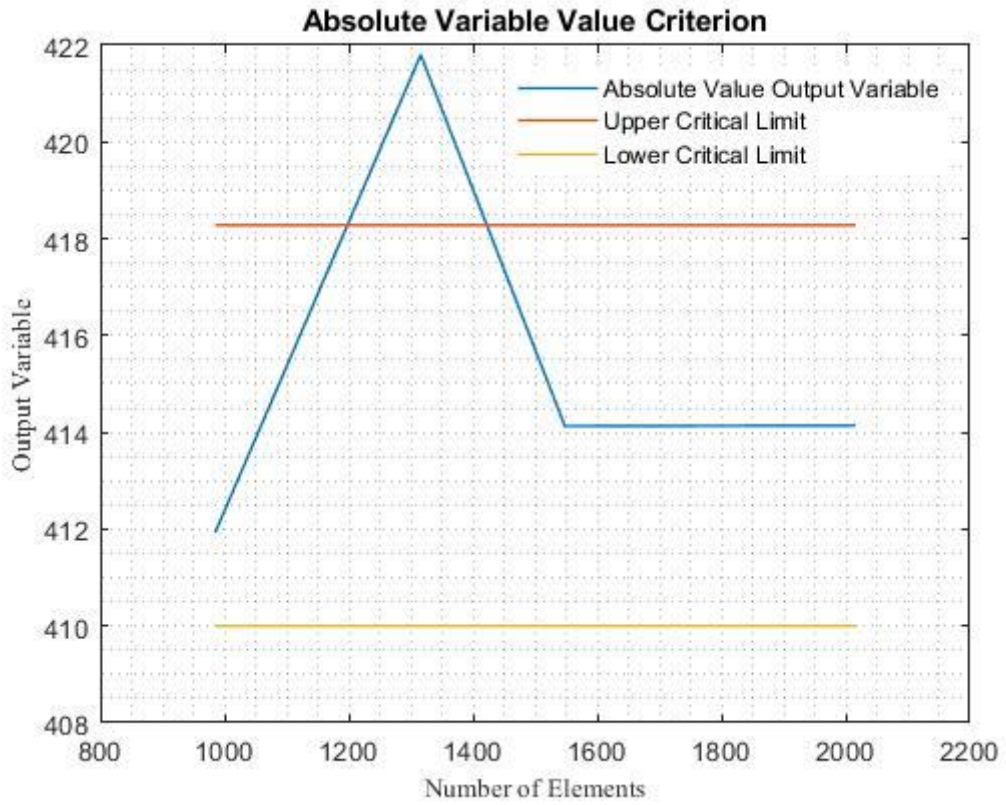

Figure 34- Absolute Value of Maximum von Mises Equivalent Stress vs Number of Vane Elements

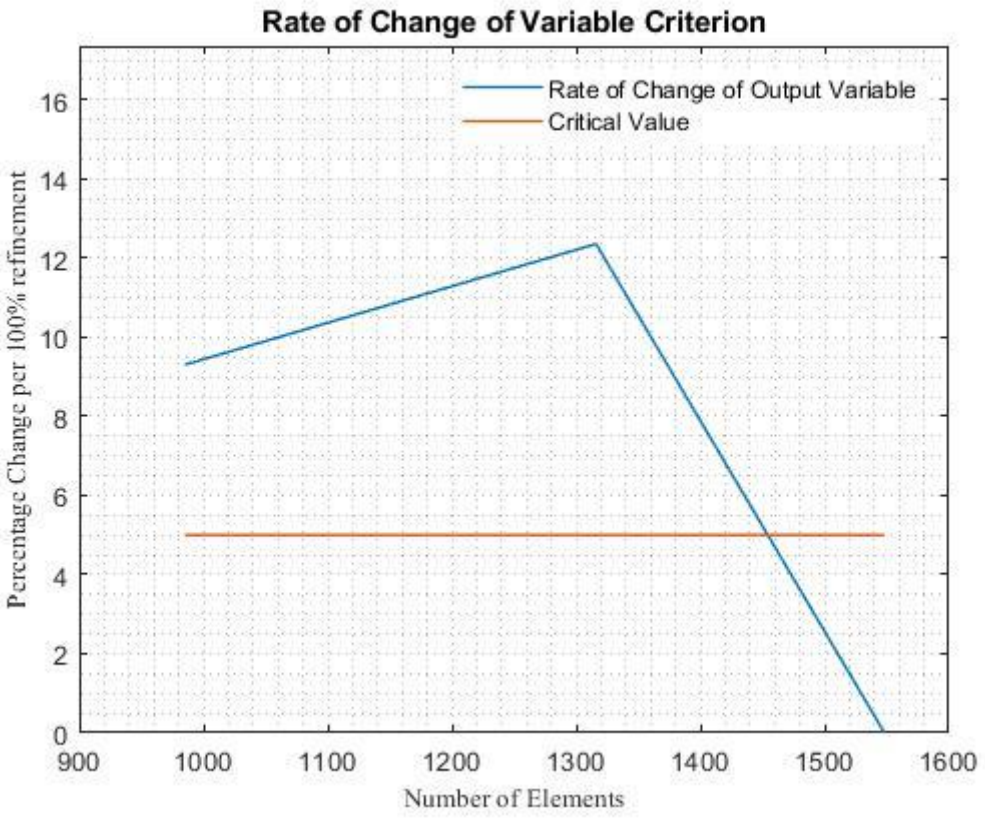

Figure 35- Percentage Rate of Change of Maximum von Mises Equivalent Stress vs Number of Vane Elements

The results show that stress convergence is achieved at approximately 1450 vane elements. This means that discretisation of the sealing vane is sufficient to capture the point of maximum stress due to the contact load.

Local Refinement Study- Vane Contact Surface

The final, and expected to be the most difficult, local refinement study to be completed was the vane contact surface study. Due to the large percentage rate of change of contact pressure in the global refinement study, the model was refined significantly to attempt to achieve contact convergence. The results of the study are shown in Figure 36 to Figure 39.

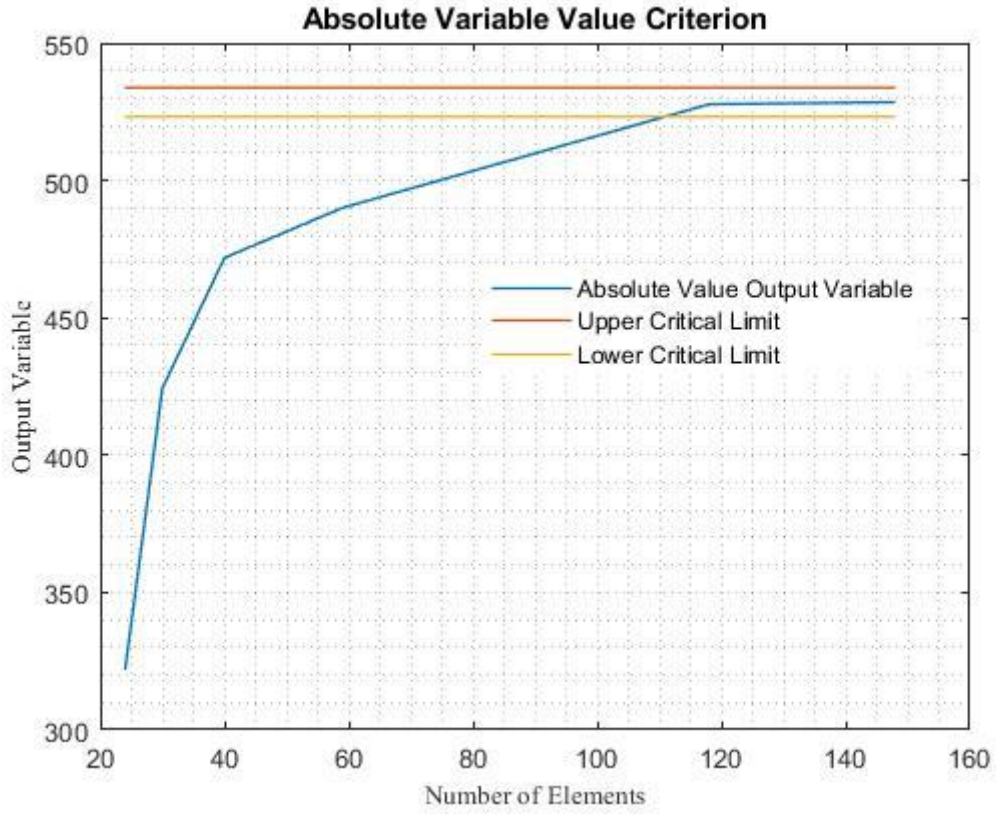

Figure 36- Absolute Value of Contact Pressure vs Number of Vane Contact Elements

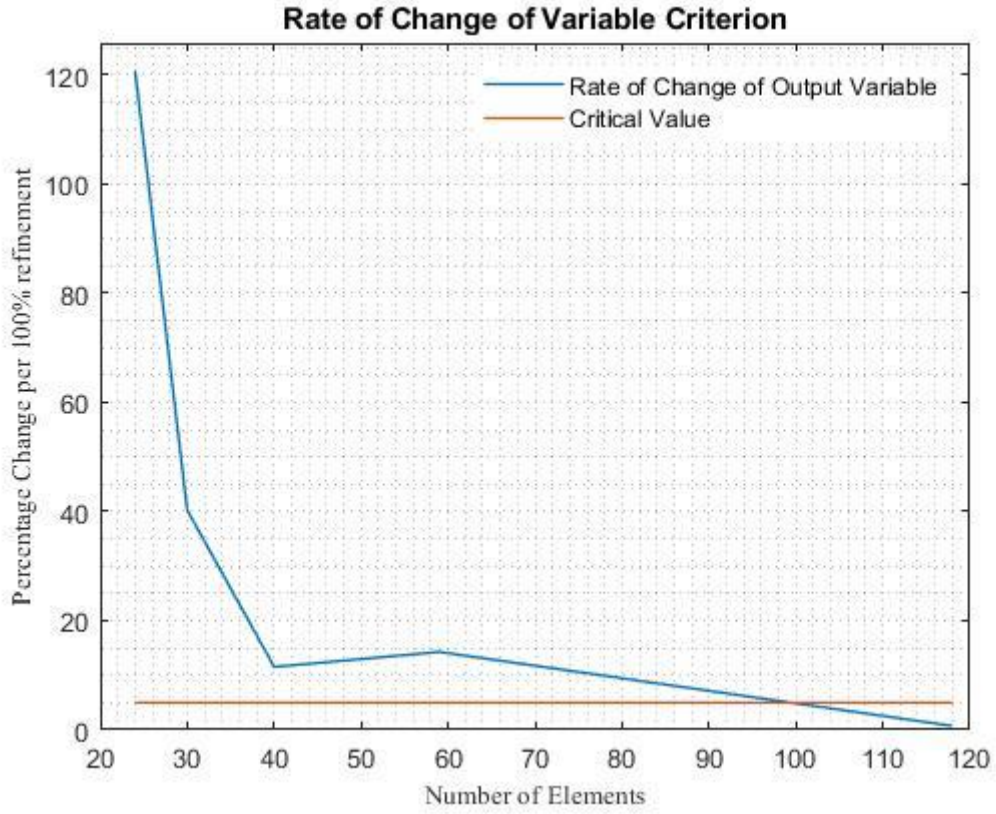

Figure 37- Percentage Rate of Change of Contact Pressure vs Number of Vane Contact Elements

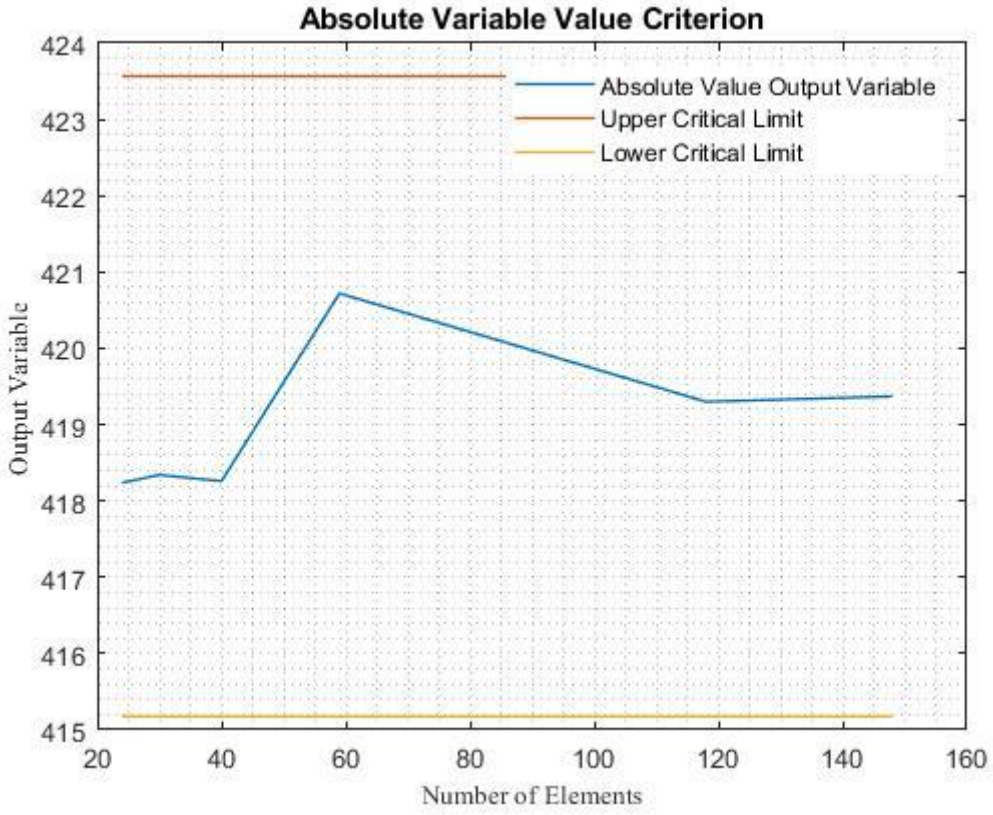

Figure 38- Absolute Value of Steady State Maximum von Mises Equivalent Stress vs Number of Vane Contact Elements

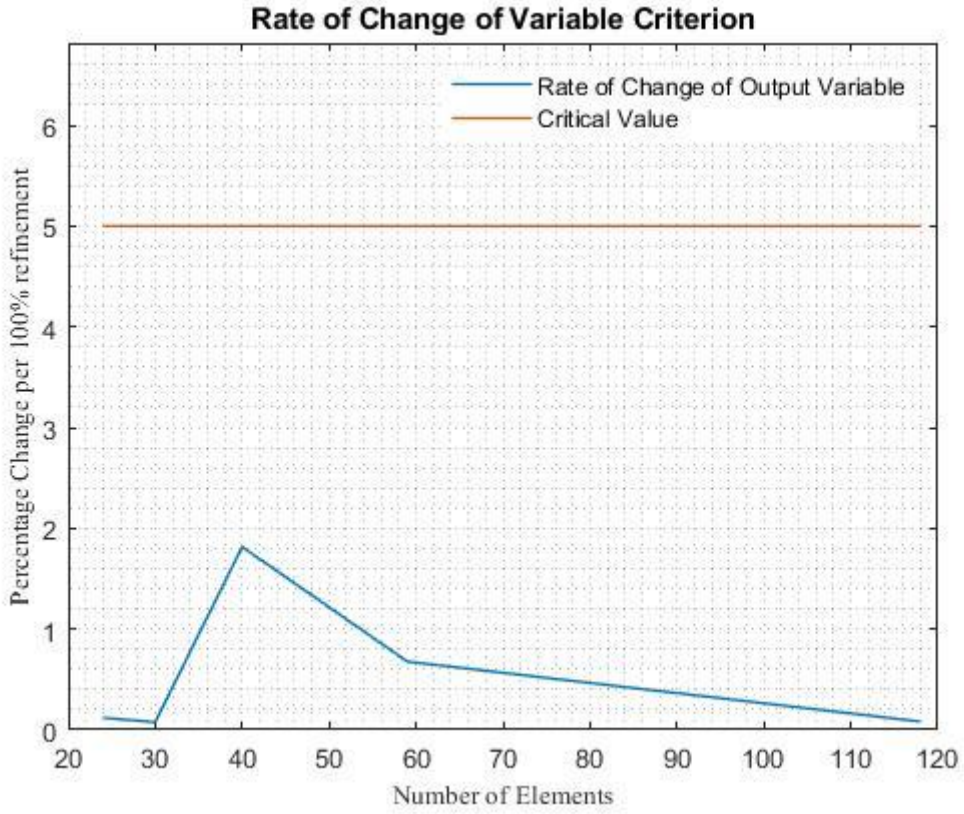

Figure 39- Percentage Rate of Change of Steady State Maximum von Mises Equivalent Stress vs Number of Vane Contact Elements

Contact convergence of the model occurred at around 100 vane contact elements. Stress convergence occurred at a comparatively low 24 elements.

Discussion

As all 3 local refinement studies were successful in achieving stress and/or contact convergence, the model was deemed to be suitably robust to continue with design optimisation. However, considering the computational time for the fully converged simulation as shown in FIGURE.

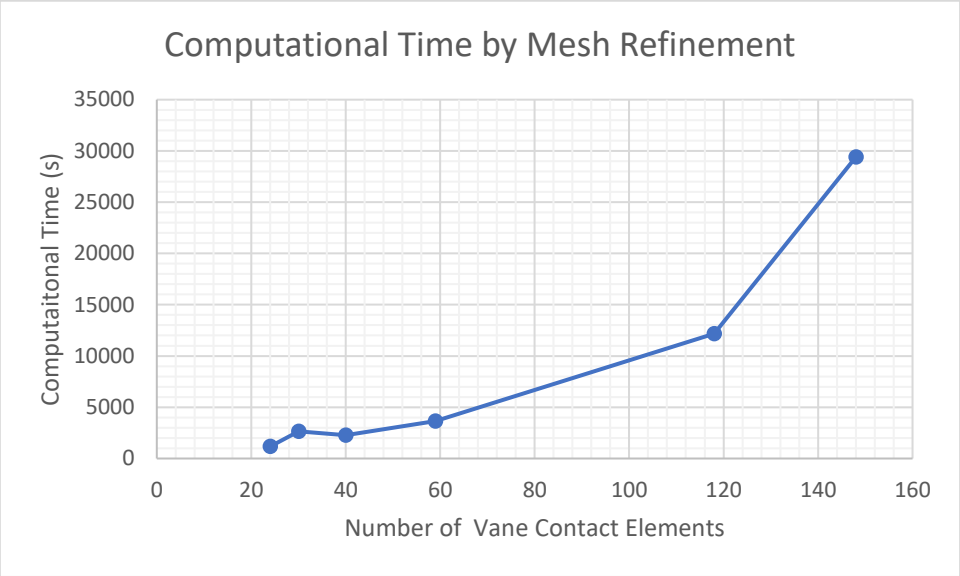

Figure 40- Computational Time by Mesh Refinement

The converged simulation was expected to take 3 hours to complete. Due to the lack of high-power computing in the project, it was decided that this model would not be feasible for use in the design optimisation section of the report. Instead, a less refined simulation, which was converged in terms of stress, but not in terms of contact pressure, was to be used. This simulation had an estimated computational time of 19 minutes- making it far more feasible for the design optimisation to be completed in the project timeline.

Steady State Design Optimisation

Once the initial simulation had been setup and its validity checked, the vane was to be optimised to meet the design purpose of the component. This was done using the surface response optimisation tool in ANSYS Design XPlorer as this was a program which the author was very familiar, and it allowed the optimisation to be done in the same program as the simulations.

Method

The parameters which were to be optimised are shown in Figure 41 and the upper and lower bounds of those parameters, shown in Table 7, were considered based on the initial simulation.

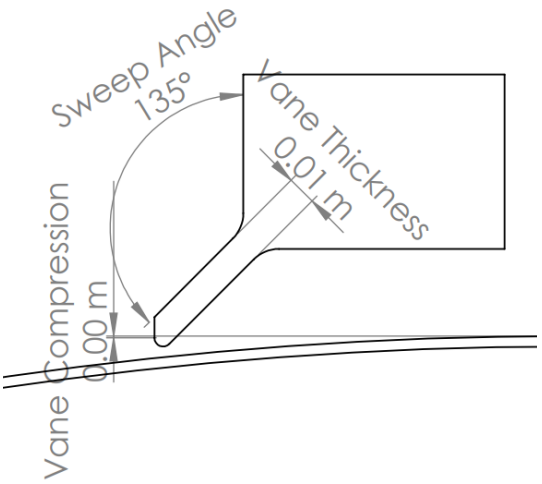

Figure 41- Geometry Optimisation Parameters of Sealing Vane

Table 7- Surface Response Optimisation Iteration 1 Input Parameter Bounds

Parameter	Lower Bound	Upper Bound
Initial Shear Modulus	500 kPa	5 MPa
Vane Sweep Angle	120 degrees	150 degrees
Vane Compression	0.002 m	0.005 m
Vane Thickness	0.01 m	0.015 m

A design of experiments was created using these values, with a composite cubic structure being used with a face centred method to efficiently order the parametric simulations to get a high-quality surface response with as little computational cost as possible.

The surface response was then generated using the in-built genetic aggregation algorithm. The response surface results were then used to determine the overall trends between the different input parameters and the relevant output parameters.

A design optimisation was then completed using a MOGA algorithm in-built to Design XPlorer. The optimisation was set up with goals as shown in Table 8.

Table 8- Optimisation goals

Parameter	Objective			Constraint	
	Goal	Target	Tolerance	Target	Tolerance

Steady State Maximum Contact Pressure	Seek Target	205 kPa	100 Pa	Above 200kPa	100 Pa
Steady State Maximum von Mises Equivalent Strain	Minimise	0.001	N/A	N/A	N/A

The goal of the optimisation was to generate a vane design which achieved the required contact pressure to maintain a vacuum seal between the station and tube environments while minimising the strain, and thus maximising the fatigue life, of the component.

Results

The surface response results are shown in Figure 42 to Figure 45.

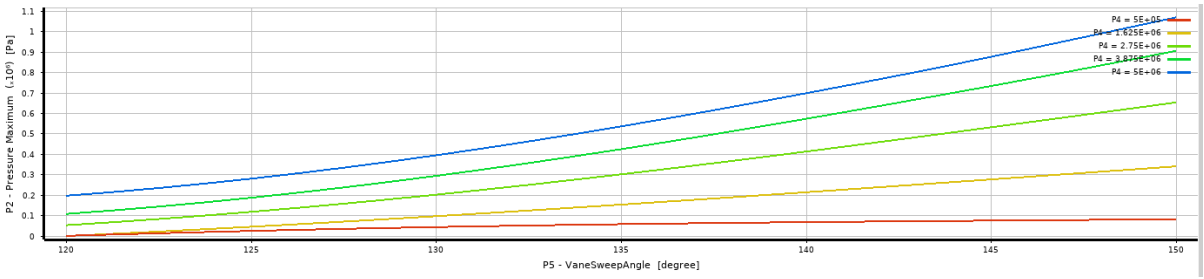

Figure 42- Vane Sweep Angle and Initial Shear Modulus vs Maximum Steady State Contact Pressure Response Surface

Figure 42 shows that the contact pressure increased by a large percentage with a relatively small increase in sweep angle. For smaller initial shear moduli, the relationship appeared to be linear. Whereas, at larger shear moduli, the relationship appeared to be more parabolic. The meant that the initial shear modulus- or physically speaking the stiffness of the vane- and the sweep angle were both effective tools for changing the contact pressure.

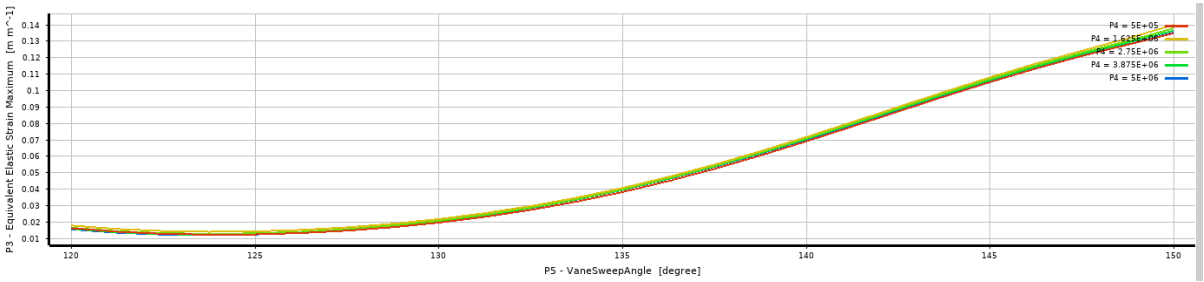

Figure 43- Vane Sweep Angle and Initial Shear Modulus vs Maximum Steady State von Mises Equivalent Strain Response Surface

Figure 43 shows that the Vane Sweep Angle significantly effected the strain in the vane. The initial shear modulus had no effect on the strain of the vane- this was expected due to the displacement-strain-stress back substitution formulation of the finite element method which meant that the stiffness parameter had no impact on the displacement or strain results. Therefore, when one is increasing the contact pressure using sweep angle, this would come at significant additional strain in the vane. Whereas increasing the contact pressure using the initial shear modulus does not come with a penalty in vane strain.

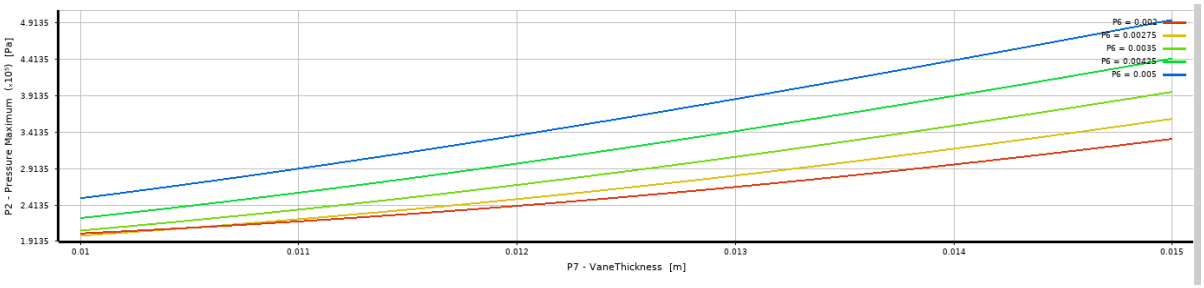

Figure 44- Vane Thickness and Vane Compression vs Maximum Steady State Contact Pressure Surface Response

Figure 44 shows that a linear relationship existed between the thickness of the vane and the maximum steady state contact pressure. An increase in contact pressure was also observed with an increase in vane compression. Both results were expected, as an increase in the volume of material and the deformation it undergoes with increase the reaction force (contact pressure) which it exerts onto the pod body.

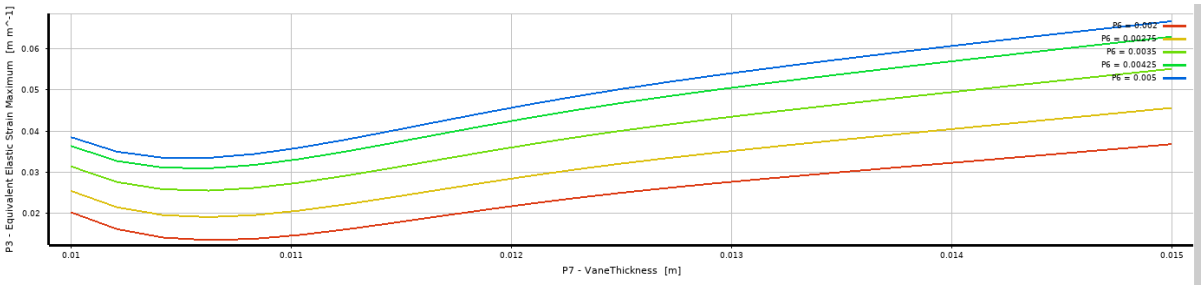

Figure 45- Vane Thickness and Vane Compression vs Maximum Steady State von Mises Equivalent Strain Surface Response

Figure 45 shows a parabolic relationship between the vane thickness and the vane strain. This result was not what was expected; however, this may have been due to a lack of resolution of the design of experiments which created an inaccurate result. The vane compression was observed to increase the sealing vane strain, with the rate of this increase decreasing as the vane compression reaches the upper bound.

From the response surfaces, it seemed like a vane with a small vane sweep angle, small vane thickness and small vane compression and a high initial shear modulus would produce optimum performance.

The candidate designs along with their validation points can be observed in Figure 46.

Name	P4 - Initial Shear Modulus Mu (Pa)	P5 - VaneSwee... (degree)	P6 - VaneComp... (m)	P7 - VaneThick... (m)	P1 - Penetration Maximum Maximum Value Over Time (m)	P2 - Pressure Maximum (Pa)		P3 - Equivalent Elastic Strain Maximum (m m^-1)	
						Parameter Value	Variation from Reference	Parameter Value	Variation from Reference
Candidate Point 1	4.5101E+06	126.98	0.0020251	0.011173	9.5492E-06	2.0499E+05	0.00%	-0.0018625	0.00%
Candidate Point 1 (verified)					6.9003E-06	2.8208E+05	37.61%	0.014095	856.80%
Candidate Point 2	4.656E+06	126.79	0.0022935	0.010741	9.2447E-06	2.0497E+05	-0.01%	-0.0017407	6.54%
Candidate Point 2 (verified) DP 2					9.2971E-06	1.3685E+05	-33.24%	0.01506	908.62%
Candidate Point 3	4.6034E+06	126.79	0.0020206	0.010879	9.2573E-06	2.0506E+05	0.04%	-0.0030464	-63.57%
Candidate Point 3 (verified)					4.5017E-06	1.5461E+05	-24.58%	0.013605	830.50%

Figure 46- Candidate Designs from Design Optimisation Iteration 1

The validation points show that the results of the optimisation were not entirely accurate. However, the candidate designs do confirm the hypothesis that a lower vane sweep angle, thickness and compression and a higher initial shear modulus produces an optimally low strain value.

Due to the poor results, the optimisation workflow was iterated with a more concentrated range of values for the optimisation parameters, shown in Table 9.

Table 9- Design Optimisation Iteration 2 Parameter Bounds

Parameter	Lower Bound	Upper Bound
Initial Shear Modulus	4 MPa	5 MPa
Vane Sweep Angle	120 degrees	130 degrees
Vane Compression	0.002 m	0.003 m
Vane Thickness	0.01 m	0.012 m

The results of this round of optimisation are shown in Figure 47 to Figure 50.

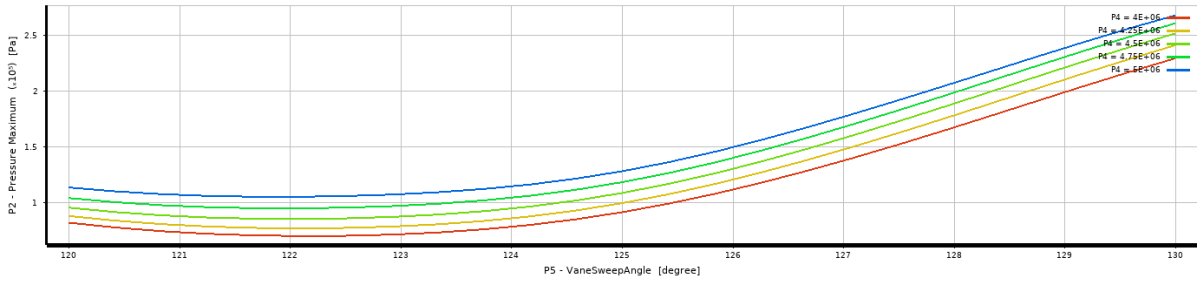

Figure 47- Iteration 2 Vane Sweep Angle and Initial Shear Modulus vs Maximum Steady State Contact Pressure

Comparing Figure 47 with Figure 42, the non-linear relationship between sweep angle and contact pressure at higher initial shear moduli is still present.

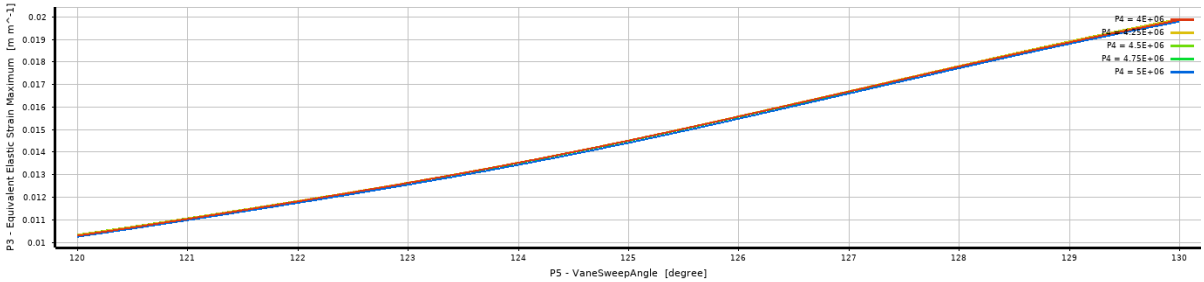

Figure 48- Iteration 2 Vane Sweep Angle and Initial Shear Modulus vs Maximum Steady State Strain

Figure 48 exhibits very different characteristics when compared to Figure 43. In this figure, the relationship between sweep angle and steady state strain is strongly linear. It should also be noted that the initial shear modulus has no effect on the steady state strain.

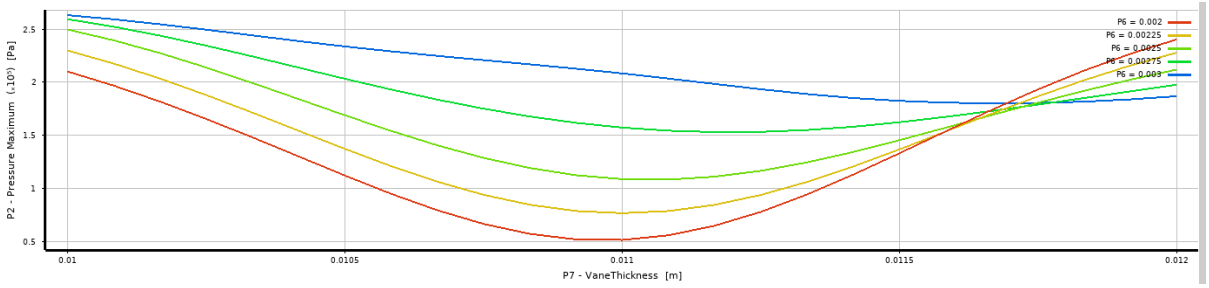

Figure 49- Iteration 2 Vane Thickness and Compression vs Maximum Steady State Contact Pressure

Comparing Figure 49 with Figure 44, the results have interestingly deteriorated from a strong linear correlation to a series of overlapping parabolic curves. The strange characteristic from this result may effect the results of the optimisation.

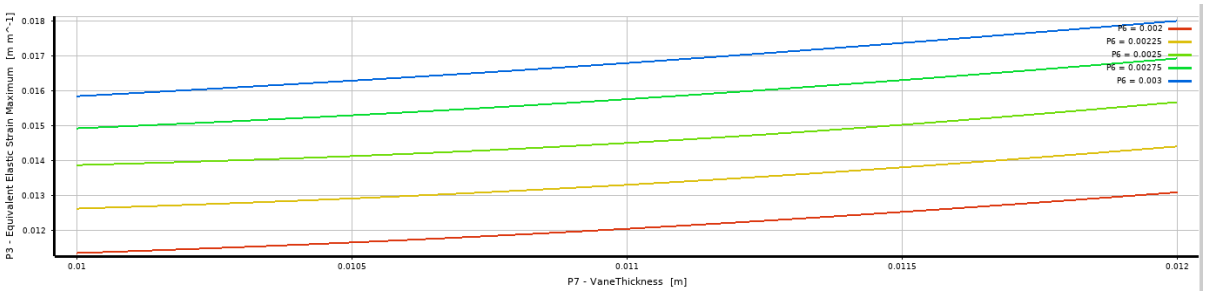

Figure 50- Iteration 2 Van Thickness and Compression vs Maximum Steady State Strain

Comparing Figure 50 to Figure 45, the results of the second iteration are far more linear between the vane thickness and steady state strain. The relationship between vane compression and steady state strain is also linear.

The optimisation was run with these new response surfaces. The generated candidate points along with a simulated verification of each point can be found in Figure 51.

Name	P4 - Initial Shear Modulus Mu (Pa)	P5 - VaneSwee... (degree)	P6 - VaneComp... (m)	P7 - VaneThick... (m)	P1 - Penetration Maximum Maximum Value Over Time (m)	P2 - Pressure Maximum (Pa)		P3 - Equivalent Elastic Strain Maximum (m m^-1)	
						Parameter Value	Variation from Reference	Parameter Value	Variation from Reference
Candidate Point 1	4.9701E+06	120	0.0022749	0.010042	8.8755E-06	2.0496E+05	-0.02%	0.0087482	-7.45%
Candidate Point 1 (verified) DP 3					1.0438E-05	2.0217E+05	-1.38%	0.0091547	-3.15%
Candidate Point 2	4.7561E+06	120	0.0020186	0.011936	5.6817E-06	2.0495E+05	-0.02%	0.0091848	-2.83%
Candidate Point 2 (verified) DP 4					5.3768E-06	1.676E+05	-18.24%	0.0099025	4.76%
Candidate Point 3	4.6862E+06	120.04	0.0024301	0.010094	9.6448E-06	2.0499E+05	0.00%	0.0094522	0.00%
Candidate Point 3 (verified) DP 5					8.6556E-06	2.1446E+05	4.62%	0.0095608	1.15%

Figure 51- Iteration 2 Optimisation Results

Candidate point 1 was the best performing point when verified; however, there was still a 4.6% increase in the steady state strain compared to the value statistically generated from the optimisation. The optimisation was to be run once more with further concentrated parameter bounds. As all candidate points used the values of sweep angle on or close to the lower bound, this value was removed from the parameter study and the value of 120 degrees was used for all simulation. The parameter bounds for iteration 3 of the parameter study are shown in Table 10.

Table 10- Iteration 3 Optimisation Parameter Bounds

Parameter	Lower Bound	Upper Bound
Initial Shear Modulus	4.5 MPa	5 MPa
Vane Sweep Angle	120 degrees	
Vane Compression	0.002 m	0.0025 m
Vane Thickness	0.01 m	0.012 m

The candidate designs generated from the optimisation algorithm are shown in Figure 52.

Name	P4 - Initial Shear Modulus Mu (Pa)	P6 - VaneCom... (m)	P7 - VaneThickness (m)	P1 - Penetration Maximum Maximum Value Over Time (m)	P2 - Pressure Maximum (Pa)		P3 - Equivalent Elastic Strain Maximum (m m^-1)	
					Parameter Value	Variation from Reference	Parameter Value	Variation from Reference
Candidate Point 1	4.7308E+06	0.0022325	0.010003	1.0594E-05	2.0506E+0	0.16%	0.0086206	0.11%
Candidate Point 1 (verified) DP 6				1.3625E-05	1.9581E+05	-4.36%	0.0088595	2.88%
Candidate Point 2	4.7521E+06	0.0022348	0.010006	1.06E-05	2.0512E+0	0.19%	0.0086233	0.14%
Candidate Point 2 (verified) DP 7				1.3083E-05	2.3536E+05	14.96%	0.0082245	-4.49%
Candidate Point 3	4.7842E+06	0.0022264	0.010001	1.0539E-05	2.0473E+0	0.00%	0.0086112	0.00%
Candidate Point 3 (verified) DP 8				1.0022E-05	1.9926E+05	-2.67%	0.0086386	0.32%

Figure 52- Iteration 3 Candidate Designs with Validation Points

All 3 candidate points show convergence towards a single design, with changes in the predicted output parameters at an order of 0.1%. The validation points showed slightly more variation, although all values of strain were close to their predicted values. In the end, candidate design 2 was chosen as the best performing design as it had the lowest value of steady state strain and the highest steady state contact pressure. Therefore, the finalised design of the sealing vane is shown in Table 11 and Figure 53.

Table 11- Finalised Sealing Vane Design

Initial Shear Modulus	Sweep Angle	Vane Compression	Vane Thickness
4.7521 MPa	120 degrees	2.2348 mm	10.06 mm

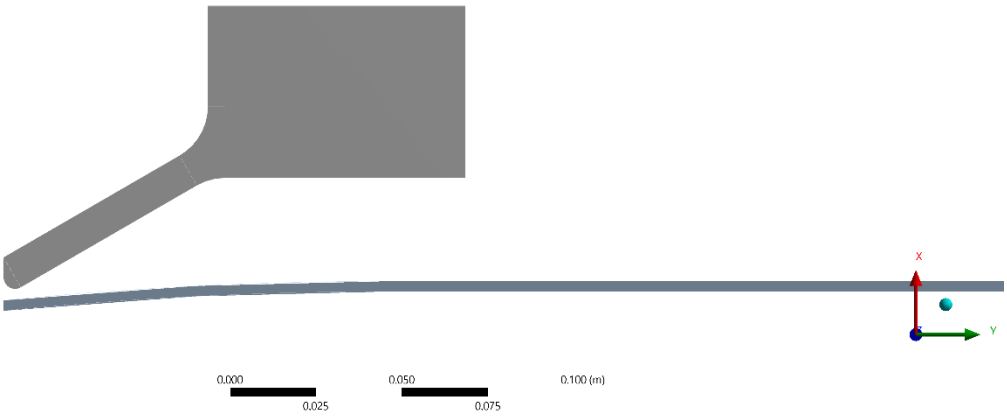

Figure 53- Optimised Vane Geometry

Discussion

Overall, the design optimisation was successful in producing a sealing vane which produced the required 200 kPa of contact pressure while minimising the strain in the component. Each iteration of optimising improved the result of the simulation, as shown by the reduction of strain in Figure 54.

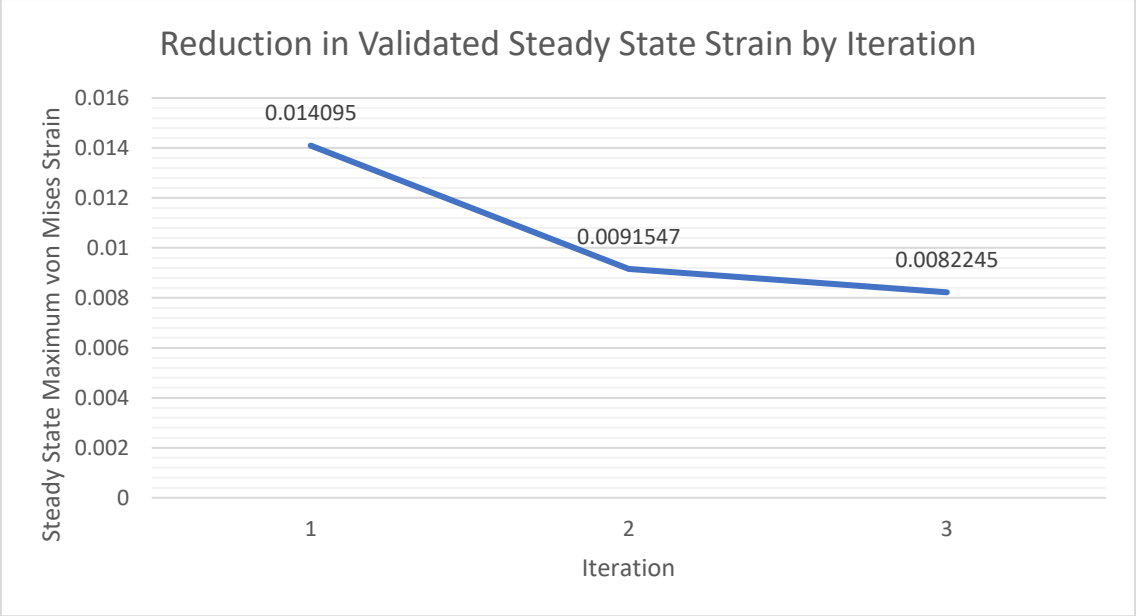

Figure 54-Reduction in Validated Steady State Strain by Iteration

The results of the new vane design is compared with the Autor's previous design produced in a previous project in Table 12.

Table 12- Previous and Current Vane Design Comparison

Performance Parameter	Minimum Steady State Contact Pressure	Maximum von Mises Equivalent Stress	Maximum Equivalent von Mises Strain	Seal Effectiveness
Old Design	224 kPa	335 kPa	0.221	0.669
New Design	235 kPa	123kPa	0.0082245	1.91

The results showed that the contact pressure and strain values were very sensitive to the sweep angle of the vane and vane thickness. The final results show both of these values should be minimised within the parameter bound, with vane stiffness and compression being used as more efficient ways of increasing contact pressure while minimising strain.

Given that the base finite element model used in these simulations was not numerically converged in terms of contact pressure, there may be some variation in the results of the optimisation with increased mesh density.

It should also be noted that the results of this optimisation aimed to find a local minimum value of strain within the original bounds of the design. There may be better performing designs out with this parameter bound, and different concepts may also be an area of future endeavours.

Sensitivity Study of Optimised Design

The optimised vane deign must be robust to varying pod velocities and friction co-efficients, as in the physical model these values may change substantially from pod to pod.

A further design of experiments was to be set up using ANSYS Design XPlorer to explore the variation in the sealing vane performance parameters with varying pod approach velocity and friction co-efficient.

Method

A custom design of experiments was setup for the design of experiments. The parameter bounds for this study are shown in Table 13.

Table 13- Parameter Bounds for Sensitivity Study

Parameter	Lower Bound	Upper Bound
Pod Approach Velocity	2.5 m/s	7.5 m/s
Co-efficient of Friction	0.1	0.3

The results of the simulation were used to create surface response graphs using an in-built genetic aggregation algorithm, similar to the design optimisation workflow.

Sensitivity of Co-Efficient of Friction

The friction sensitivity plots are shown in Figure 55 and Figure 56.

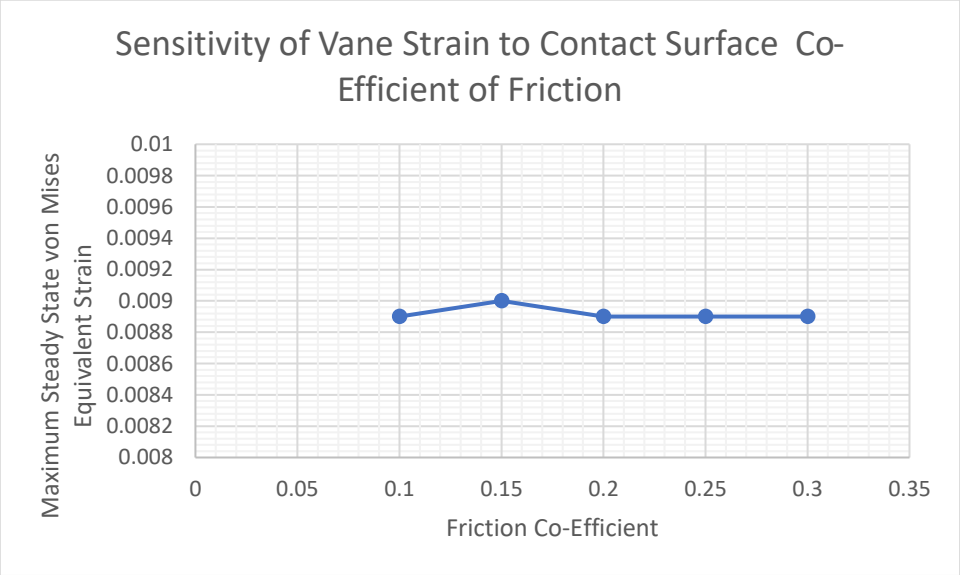

Figure 55- Friction Co-Efficient Sensitivity of Vane Strain

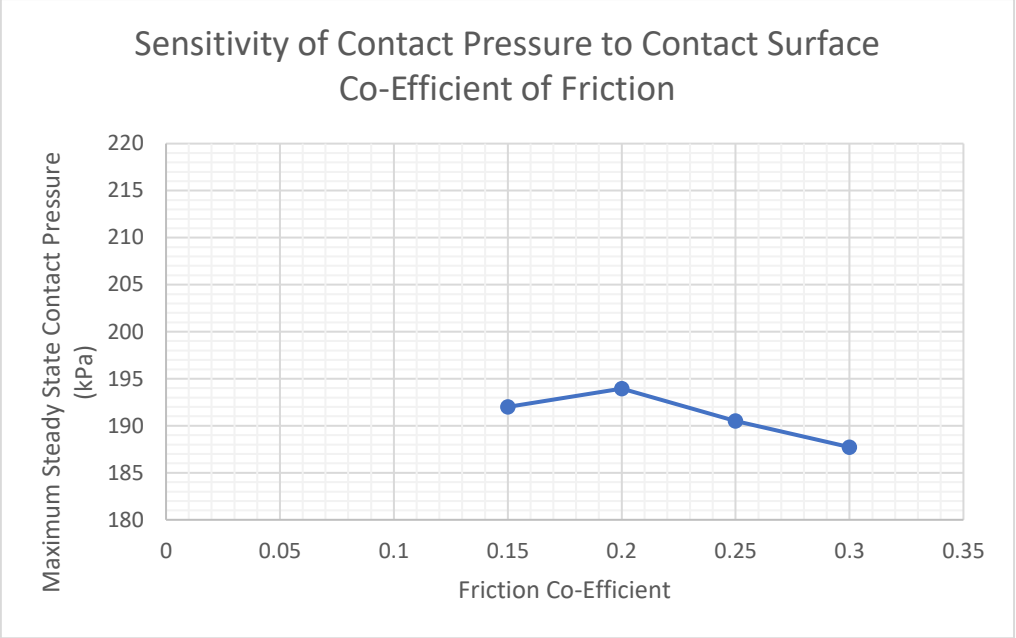

Figure 56- Friction Sensitivity of Vane Contact Pressure

Sensitivity of Pod Approach Velocity

The pod velocity plots are shown in Figure 57 and Figure 58.

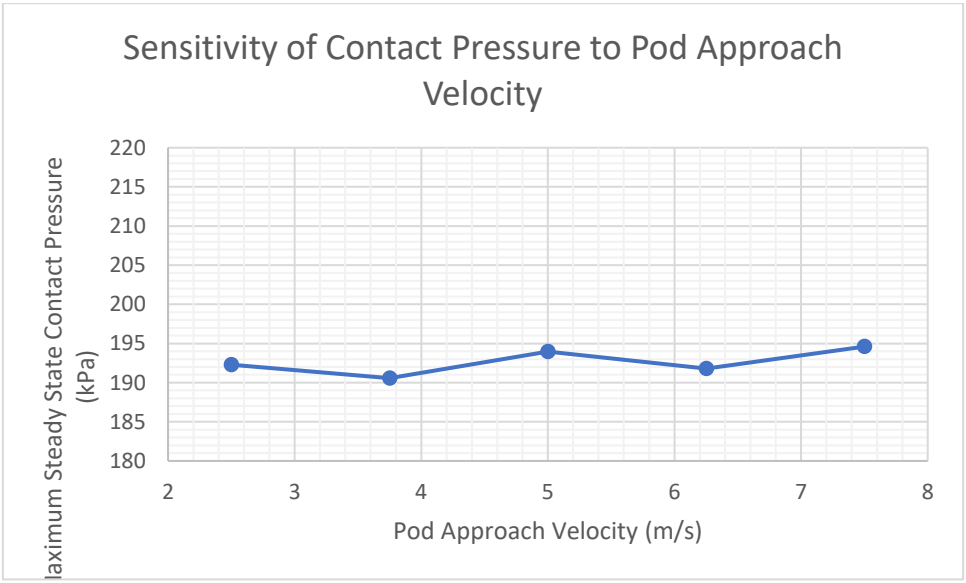

Figure 57- Pod Velocity Sensitivity of Vane Contact Pressure

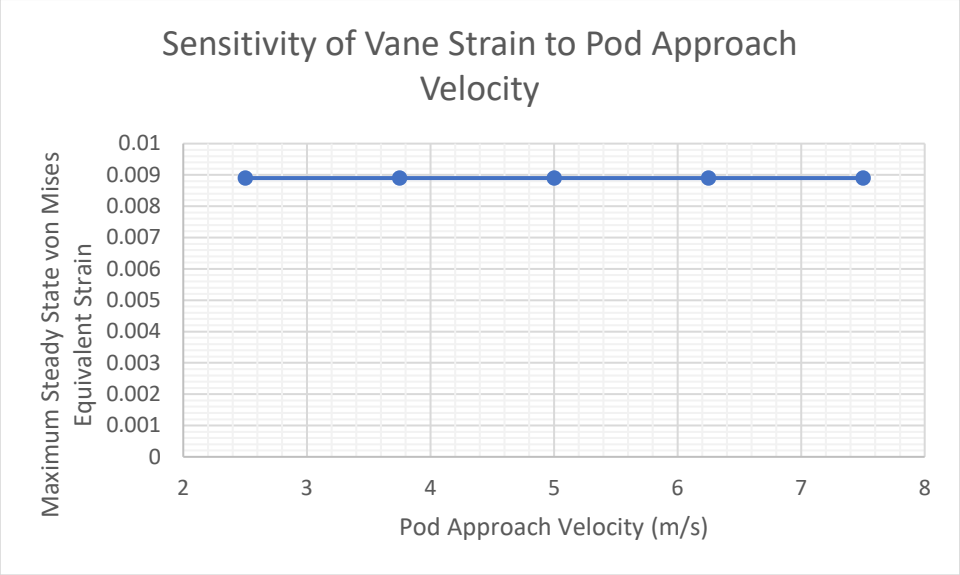

Figure 58- Pod Velocity Sensitivity of Vane Strain

Discussion

Figure 55 and Figure 58 show that the steady state strain in the sealing vane is not very sensitive to changes in friction co-efficient or pod velocity. This means that the pod can approach at slightly varying speeds without detrimentally impacting the lifespan of the vane component.

Figure 56 and Figure 57 showed that the pod velocity and friction co-efficient had no effect on the steady state contact pressure of the sealing vane. This means that changes to these parameters in the physical model will not affect the vane's ability to provide the required contact pressure to create a seal between the two different environments.

As some of the simulations with higher velocities and friction co-efficients did not reach a steady state during the simulated time, a settling time MATLAB code was used to statistically derive this value based on the average of the last 50 output performance variable values in the simulated time range. This may have caused some inaccuracies in the results, which is showed by the reduced pressure and increased strain results of the standard value simulations.

Final Discussion

Referring to the project initial outcomes, significant areas of the initial scope were not completed. This was mainly due to a lack of compatibility with contact pressure results when creating a 2-dimensional model using the LS-DYNA plugin on ANSYS workbench. Several attempts were made at finding a solution to this incompatibility, to no avail. Upon reflection, LS-DYNA is a specialist 3-dimnesional finite element software which is incredibly powerful for impacts and collision testing. However, for the case studied in this project it showed clear limitations in dealing with the challenges of a 2-dimensional axisymmetric model with complex contact phenomena. ABAQUS explicit may be a more appropriate software for any future work. Unfortunately, tuition in this software was not within the scope of the project when these details came to the fore.

Significant strides were made in the improvement of the quality of the Implicit finite element model, this is shown by the achievement of full convergence of stress and contact pressure in the model. The increase in pod approach velocity to 5 m/s also increases the maximum potential throughput of the airlock. However, a shorter lever time gate valve would be required to reduce the air leakage per cycle of the airlock.

Design optimisation using ANSYS design XPlorer significantly improved the effectiveness of the sealing vane; and thus, the expected fatigue life of the sealing vane. The lack of high-power computing hindered the quality of these results in two ways. Firstly, the fully converged version of the finite element model could not be used for the optimisation due to time constraints. Secondly, the number of simulations and iterations which could be completed within the project timeframes. However, the quality of the results is sufficient for improvements to the sealing to have been made.

The sealing vane showed a good robustness to changes in the pod approach velocity and friction co-efficient. This means that the designed sealing vane will still be able to perform as expected as these parameters vary in the physical model. It should also be noted that more finite element modelling, and physical testing will be needed to validate these claims, as the results of this study were statistical, not directly numerical.

Future Work

Despite the success of the design optimisation in improving the sealing vane design, there are several avenues for development for both the sealing vane component and the wider Hyperloop airlock concept.

1. Completing the design optimisation with the fully converged version of the finite element model and a larger input parameter bound to produce a design which is more physically valid (using high power computing).
2. Physical experimentation and prototyping to confirm the results generated from the finite element model.
3. Using of ABAQUS Explicit or another Explicit program to further analyse the impact response of the sealing vane component.
4. Design of a short lever time gate valve to reduce the air leakage through the airlock per pod cycle at the new, increased pod approach velocity.
5. Development of a fully 3-dimensional sealing vane design around a full Hyperloop pod concept.

Closing Remarks

The project had to be incarnated several times over the duration of working on it; however, key progress was still made, and new understanding developed.

ANSYS workbench was used to make an implicit transient finite element model of the pod body impacting the sealing vane.

This model was then verified using a mesh refinement study.

ANSYS Design XPlorer was then used to optimise the sealing vane parameters to maximise the lifespan of the component while still performing as expected.

A sensitivity study was conducted to find that the final vane design is robust to changes in pod approach velocity and friction co-efficient.

While an outright claim of feasibility could not be made in this project, the improvement of the sealing vane design takes an important step forward for this concept as a part of Hyperloop's future.

Acknowledgements

The author would like to thank the following people:

- Dr Stephen Connolly for his supervision and guidance through the many twists and turns of the project, and for providing computer access throughout the project.
- Dr Yevgen Gorash for his consultation on the finite element modelling phase of the project.
- Gregor McInnes, Dillon Bradley, and Elizabeth Jennings of Strathloop for their support on a personal front throughout the project timeframe.

Lastly, a big thank you to the Department of Mechanical and Aerospace Engineering at the University of Strathclyde for providing infrastructure and the Carnegie Trust Fund for Universities in Scotland for financially supporting this project.

References

[1] H.-H. Lee, *Finite Element Simulations with ANSYS Workbench 14*. 2012.

[2] L. Shi, “Analysing Elastomer Automotive Body Seals Using LS-DYNA,” in *7th International LS-DYNA Users Conference*, pp. 21–30, [Online]. Available: https://www.dynalook.com/conferences/international-conf-2002/Session_4-4.pdf.

[3] T. Schmidt, M. Andre, and G. Poll, “A transient 2D Finite Element Approach for the simulation of mixed lubrication effects of reciprocating Hydraulic Rod Seals,” *Tribol. Int.*, vol. 43, pp. 1775–1785, 2010.

[4] A. Thatte and R. F. Salant, “Visco-elastohydrodynamic model of a hydraulic rod seal during transient operation,” *J. Tribol.*, vol. 132, no. 4, 2010, doi: 10.1115/1.4002542.

[5] A. Thatte and R. F. Salant, “Transient EHL analysis of an elastomeric hydraulic seal,” *Tribol. Int.*, vol. 42, pp. 1424–1432, 2009.

[6] F. J. Martínez, M. Canales, S. Izquierdo, M. A. Jiménez, and M. A. Martínez, “Finite element implementation and validation of wear modelling in sliding polymer-metal contacts,” *Wear*, vol. 284–285. pp. 52–64, 2012, doi: 10.1016/j.wear.2012.02.003.

[7] Y. Gorash, A. Bickley, and F. Gozalo, “Application of the Cel Approach To Consider Fsi for the Assessment of Leak Tightness for Elastometric Seals,” 2018.

[8] N. Morrison, Y. Gorash, and R. Hamilton, “COMPARISON OF SINGLE-SOLVER FSI TECHNIQUES FOR THE FE- PREDICTION OF A BLOW-OFF PRESSURE FOR AN ELASTOMERIC SEAL,” in *European Conference on Computational Mechanics*, 2018, no. June, pp. 11–15.

[9] N. Morrison, Y. Gorash, and R. Hamilton, “Assessment of leak tightness for swellable elastomeric seals considering fluid-structure interaction with the CEL approach,” 2018.

[10] B. Yang and R. F. Salant, “A numerical model of a reciprocating rod seal with a secondary lip,” *Tribol. Trans.*, vol. 51, no. 2, pp. 119–127, Mar. 2008, doi: 10.1080/10402000701691746.

[11] A. Ali, M. Hosseini, and B. B. Sahari, “A review and comparison on some rubber elasticity models,” *J. Sci. Ind. Res. (India).*, vol. 69, no. 7, pp. 495–500, 2010.

[12] B. Kim *et al.*, “A comparison among Neo-Hookean model, Mooney-Rivlin model, and Ogden model for Chloroprene rubber,” *Int. J. Precis. Eng. Manuf.*, vol. 13, no. 5, pp. 759–764, 2012, doi: 10.1007/s12541-012-0099-y.

[13] J. D. Ferry, *Viscoelastic Properties of Polymers*. 1980.

[14] M. Kaliske and H. Rothert, “Formulation and implementation of three-dimensional viscoelasticity at small and finite strains,” *Comput. Mech.*, vol. 19, no. 3, pp. 228–239, 1997, doi: 10.1007/s004660050171.

[15] T. Chen, “Determining a Prony Series for a Viscoelastic Material From Time Varying Strain Data,” 2000. [Online]. Available: http://www.sti.nasa.gov.

[16] J. E. Soussou, F. Moavenzadeh, and M. H. Gradowczyk, “Application of Prony Series to Linear Viscoelasticity,” *Trans. Soc. Rheol.*, vol. 14, no. 4, pp. 573–584, Dec. 1970, doi: 10.1122/1.549179.

[17] J. E. L. Pacheco, C. A. Bavastri, and J. T. Pereira, “Viscoelastic relaxation modulus characterization using Prony series,” *Lat. Am. J. Solids Struct.*, vol. 12, no. 2, pp. 420–445,

2015, doi: 10.1590/1679-78251412.

[18] W. M. L, R. F. Landel, and J. D. Ferry, “The Temperature Dependence of Relaxation Mechanisms in Amorphous Polymers and Other Glass-forming Liquids,” vol. 679, no. 12, 1955.

[19] D. W. Aubrey and M. Sherriff, “Viscoelasticity of Rubber-Resin Mixtures,” *J. Polym. Sci.*, vol. 16, pp. 2631–2643, 1978.

[20] P. A. Ciullo and N. Hewitt, *THE RUBBER FORMULARY*. 1999.

[21] A. D. Drozdov, “A constitutive model for nonlinear viscoelastic media,” *Int. J. Solids Struct.*, vol. 34, pp. 2685–2707, 1997.

[22] J. Małachowski, J. Bukala, K. Damaziak, and M. Tomaszewski, “Ls-Dyna Contact Procedure Analysis for Selected Mechanical Systems,” *J. KONES. Powertrain Transp.*, vol. 22, no. 1, pp. 193–202, 2015, doi: 10.5604/12314005.1161741.

[23] Z. Yang, X. Deng, and Z. Li, “Numerical modeling of dynamic frictional rolling contact with an explicit finite element method,” *Tribology International*, vol. 129. pp. 214–231, 2019, doi: 10.1016/j.triboint.2018.08.028.

[24] V. L. Popov, M. Heß, and E. Willert, *Handbook of Contact Mechanics*. 2019.

Appendix

Mesh Convergence MATLAB Code

```
clc
clear all
close all

n= [24, 30, 40, 59, 118, 148];
s= [321.8, 424.34, 471.84, 490.04, 527.72, 528.49];
RC= 0.05;
AV= 0.02;
trigger =0;
dnn= n(end)-n(1);

if size(n,1)~=1 || size(s,1)~=1
    disp('Input Error: Inputs as 1 x m matrix');
    return
end

if RC>0.1
    disp('Consider reducing relative convergence factor, RC, below 0.1');
elseif RC<0.01
    disp('Consider increasing relative convergence factor, RC, above
0.01');
end

if AV>0.05
    disp('Consider reducing absolute value factor, AV, below 0.05');
elseif AV<0.001
    disp('Consider increasing the absolute value factor, AV, above 0.01');
end

for d= 1:1:size(n,2)
    if n(d)<0
        disp('Error in Input: Negative Number of Elements');
        return
    elseif d>1
        if n(d)<n(d-1)
            disp('Input Error: Please Insert Number of Elements Array in
Ascending Order');
            return
        end
    end
end

if dnn<1
    disp('Mesh Refinement Steps May be too small to verify convergence:
Consider using larger refinement steps');
end

if size(n,2)~=size(s,2) || size(n,1)~=size(s,1)
    disp('Invalid Inputs! Ensure Input Matrices are same length');
    return
end

sf= s(end);
nf= n(end);
```

```
for i= 2:1:size(s,2)
    disp('_____________________________');
    X= ['Checking Convergence at ', num2str(n(i-1)), ' elements'];
    disp(X);
   s_upper(1)= (1+AV)*sf;
   s_lower(1)= (1-AV)*sf;
   s_upper(i-1)= (1+AV)*sf;
   s_lower(i-1)= (1-AV)*sf;
   crit(i-1)= RC;
   dsdn_(i-1)= ((s(i)-s(i-1)))/(s(i))/((n(i)-n(i-1))/(n(i)));
   dsdn(i-1)= abs(dsdn_(i-1));
   dn(i-1)= abs((n(i)-n(i-1))/n(i));
   if dn(i-1)<=0.2
            disp('WARNING not enough percentage mesh refinement to guarantee
convergence at this point');
   end
   if dsdn(i-1)<=RC && trigger==0
       if s(i-1)>=s_upper(1,i-1) && s(i-1)<=s_lower(i-1)
           disp('WARNING Absolute Convergence Factor out of Tolerance Out
of Tolerance at this point')
       end
       X= ['Converged Solution at ', num2str(n(i-1)), ' elements'];
       disp(X);
       if i==2
           disp('Error in finding intercept value');
       else
       disp(X);
       trigger= 1;
       r= i-1;
       [p,q]= my_polyxpoly(n(1:r),dsdn,n(1:r),crit(1:r),1e-03);
       p= ceil(p);
       if p>0
           for l= 1:1:size(n,2)
               if n(l)== p
                   X= ['Convergnece occuring exactly on ', num2str(n(l)), '
elements'];
                   disp(X);
                   break
               elseif l==size(n,2)
                   X= ['Try a simulation with ', num2str(p), ' elements'];
       disp(X);
               end
               end
       else
           disp('Error finding intercept value');
       end
       end
   else
               disp('No Convergence at this point');
   end
end
s_upper(i)= (1+AV)*sf;
s_lower(i)= (1-AV)*sf;
N= n(1:end-1);
DSDN= dsdn.*100;
CRIT= crit.*100;
E= diff(dsdn_);
if abs(E(end)/E(end-1))>1.5
    disp('Potential Stress Singularity or Contact Bounce Issue: Check Point
of Maximum Stress');
```

```
elseif dsdn_(end)*dsdn_(end-1)<0
        disp('Unstable mesh convergence: check FE model');
end

if s(1)>s_lower(1) && s(1)<s_upper(1)
    disp('Mesh is likely over refined, consider reducing refinement');
end

if mean(s)>(1+(AV/5))*sf && mean(s)<(1-(AV/5))*sf
    disp('It may be that areas of mesh refinement are not impacting output
variable: Check FE model');
end

figure1= figure;
axes1= axes('Parent', figure1);
box(axes1,'on');
grid(axes1,'minor');
hold(axes1,'all');
ylim([0, max(DSDN)+5]);
xlabel('Parent', axes1,'Number of Elements','FontSize',10,'FontName','Times
New Roman');
ylabel('Parent', axes1,'Percentage Change per 100%
refinement','FontSize',10,'FontName','Times New Roman');
plot1 = plot(N, DSDN, N, CRIT, 'Parent',axes1,'LineWidth',1);
legend('Rate of Change of Output Variable', 'Critical Value');
title('Rate of Change of Variable Criterion');

figure2= figure;
axes2= axes('Parent', figure2);
box(axes2,'on');
grid(axes2,'minor');
hold(axes2,'all');
xlabel('Parent', axes2,'Number of Elements','FontSize',10,'FontName','Times
New Roman');
ylabel('Parent', axes2,'Output Variable','FontSize',10,'FontName','Times
New Roman');
plot2 = plot(n, s, n, s_upper, n, s_lower, 'Parent',axes2,'LineWidth',1);
legend('Absolute Value Output Variable', 'Upper Critical Limit', 'Lower
Critical Limit');
title('Absolute Variable Value Criterion');
```